m^{6}A modification controls the innate immune response to infection by targeting type I interferons

m^6A modification controls the innate immune response to infection by targeting type I interferons

Roni Winkler[1], Ella Gillis[1], Lior Lasman[1], Modi Safra[1], Shay Geula[1], Clara Soyris[1], Aharon Nachshon[1], Julie Tai-Schmiedel[1], Nehemya Friedman[2,3], Vu Thuy Khanh Le-Trilling[4], Mirko Trilling[4], Michal Mandelboim[2,3], Jacob H. Hanna[1], Schraga Schwartz[1] and Noam Stern-Ginossar[1*]

[1] Department of Molecular Genetics, Weizmann Institute of Science, Rehovot, Israel.

[2] Central Virology Laboratory, Ministry of Health, Chaim Sheba Medical Center, Ramat-Gan, Israel.

[3] Department of Epidemiology and Preventive Medicine, School of Public Health, Sackler Faculty of Medicine, Tel-Aviv University, Tel-Aviv, Israel.

[4] Institut für Virologie, Universitätsklinikum Essen, Universität Duisburg-Essen, Essen, Germany.

* To whom correspondence should be addressed: noam.stern-ginossar@weizmann.ac.il

ABSTRACT

N^6-methyladenosine (m^6A) is the most common mRNA modification. Recent studies revealed that depletion of m^6A machinery leads to alterations in the propagation of diverse viruses. These effects were proposed to be mediated through dysregulated methylation of viral RNA. Here we show that following viral infection or stimulation of cells with an inactivated virus, the deletion of m^6A 'writer', METTL3, or 'reader', YTHDF2, led to an increase in the induction of interferon-stimulated genes. Consequently, propagation of different viruses was suppressed in an interferon signaling dependent manner. Significantly, the mRNA of *IFNB*, the main cytokine that drives type I interferon response, was m^6A-modified, and was stabilized upon repression of METTL3 or YTHDF2. Furthermore, we show that m^6A-mediated regulation of interferon genes was conserved in mouse. Altogether, our findings uncover the role of m^6A as negative regulator of interferon response, by dictating the fast turnover of interferon mRNAs and consequently facilitating viral propagation.

INTRODUCTION

Methylation at the N^6 position of adenosine (m^6A) is the most abundant internal mRNA modification, which is present in over 25% of human transcripts and typically enriched near stop codons and terminal exons[1–3]. It has been linked to various stages along the post-transcriptional trajectory of mRNA, and in particular to promoting mRNA decay[3–8]. Deposition of m^6A occurs co-transcriptionally through a large protein complex ('m^6A writers'), comprising the catalytic subunit METTL3 and co-factors such as METTL14 and WTAP[8–10]. The modification is then functionally 'interpreted' through the binding of m^6A 'reader' proteins, which multiple of them have been identified. Among m^6A 'readers', the cytoplasmic YTH-domain family 1 (YTHDF1), YTHDF2 and YTHDF3 proteins have been shown to directly bind and recognize m^6A through their C-terminal YTH domain. These proteins are thought to mediate a myriad of cellular processes including mRNA decay[8] and it has been recently proposed that m^6A and its YTHDF 'readers' play a central role in shaping the cellular 'identity' by regulating a synchronized processing of groups of transcripts[11]. Finally, two potential demethylase 'erasers' (ALKBH5 and FTO) were suggested to remove m^6A modification from mRNAs[12–14].

Functionally, m^6A has been shown to impact fundamental cellular processes in diverse organisms, including meiosis[15], circadian clock[16], DNA damage repair[17], differentiation of embryonic stem cells[18], sex determination and neuronal functions[19]. More recent *in vivo* studies conducted in mice uncovered deficits in differentiation[20,21] and in immune homeostasis[22,23] in mice deficient in m^6A machinery proteins. These studies have established critical roles for m^6A-dependent mRNA decay in regulating cellular machineries[10].

The presence of m^6A on transcripts of diverse viruses has long been known (reviewed in [24]). The identification of the m^6A machinery components stimulated new research into the roles of m^6A modification in viral RNA processing. Recent studies demonstrated that m^6A 'writers' and 'readers' play important roles in modulating the life cycle of numerous RNA and DNA viruses[25–34]. Although in most of these studies the mechanistic basis of m^6A effects on viral propagation remained unclear, in all studies viral mRNAs were shown to be m^6A-modified and m^6A effects were suggested to occur by direct m^6A-mediated regulation of viral RNA processing.

Here we reveal that upon depletion of the m^6A 'writer' METTL3, viral infection resulted in a modular and highly-specific induction of hundreds of interferon-stimulated genes

(ISGs), which constitute one of the first lines of antiviral defense. Consistent with these observations, we show that drug-induced blocking of interferon (IFN) signaling restored viral proliferation in METTL3- or YTHDF2-depleted cells. Importantly, this modular ISG induction was also seen after stimulation of cells with a UV-inactivated virus, illustrating that this effect was not driven by viral mechanisms. We demonstrate that the mRNA of IFN-β, the central cytokine that drives the type I IFN response, was modified by m^6A and was significantly stabilized upon depletion of METTL3 or YTHDF2. Furthermore, m^6A methylation of *IFNB1* was conserved in murine cells and *Ifna* mRNA was also modified by m^6A. Finally, by constructing gene-deficient mice, we show that mice lacking the m^6A 'reader' protein YTHDF3 exhibit enhanced *Ifna* and *Ifnb* induction upon viral infection. Altogether, our findings highlight the central role of m^6A as negative regulator of type I IFN response, by dictating the fast turnover of *IFNA* and *IFNB* mRNAs.

RESULTS

The m^{6}A machinery is required for human cytomegalovirus propagation

The herpesvirus, human cytomegalovirus (HCMV), replicates in the nucleus relying on cellular machinery for viral gene transcription and processing. We hypothesized that m^{6}A is likely to be involved in HCMV propagation. Supporting this hypothesis, we observed that m^{6}A 'writers' and 'readers' were both transcriptionally and translationally induced along HCMV infection[35] (Supplementary Fig. 1a). We confirmed those findings in primary human foreskin fibroblasts, in which the m^{6}A 'writer' proteins METTL3 and METTL14 and 'reader' proteins YTHDF2 and YTHDC1 were upregulated by HCMV infection at the protein level (Fig. 1a). This induction of the m^{6}A machinery prompted us to examine how depletion of m^{6}A 'writers', 'readers' and 'erasers' impacts HCMV propagation. Using CRISPR/Cas9 and sgRNAs targeting the m^{6}A 'writer' proteins METTL3, METTL14 and WTAP, the m^{6}A 'reader' proteins YTHDF1, YTHDF2, and YTHDF3 or the putative m^{6}A demethylases FTO and ALKBH5, we generated fibroblasts in which these proteins were depleted. Since we used primary fibroblasts, we did not isolate single cell clones but instead we confirmed the efficient depletion of the targeted proteins in a mixed population (Supplementary Fig. 1b,c). These cells were infected with an HCMV strain containing an SV40 promoter-driven expression of green fluorescent protein (GFP)[36], which allows for fluorescence-based monitoring of infection. Supernatants were collected and used to infect fresh wild-type fibroblasts and the percentage of GFP positive cells was measured, as proxy for viral titers, by flow cytometry (Fig. 1b,c) and microscopy (Supplementary Fig. 1d). Notably, we observed strong reduction in viral titers when viruses were propagated in cells depleted of m^{6}A 'writers' or 'readers' (Fig. 1b) and elevation in viral titers when ALKBH5-depleted cells were used (Fig. 1c). These effects were not due to differences in the cells viability before or after HCMV infection (Supplementary Table 1). Furthermore, the efficiency of initial infection was comparable in wild-type and depleted cells, as we did not observe any differences in the abundance of the major immediate early viral protein (IE1-pp72) and the virally encoded GFP at 24 hours post infection (hpi) (Fig. 1d and Supplementary Fig. 1e). Significant reduction in viral protein expression was observed at 48 hpi, in cells depleted of METTL3 compared to control cells, illustrating that the block in viral propagation occurred at relatively late stages of HCMV infection (Fig. 1e and Supplementary Fig. 1f).

m^6A-mediated inhibition of HCMV growth is driven by enhanced type I IFN response

To date studies have suggested that the effect of m^6A 'writers' and 'readers' on viral propagation are mediated by methylation and dysregulation of viral transcripts[25–34]. To assess whether HCMV transcripts were m^6A-modified, we performed genome-wide m^6A methylation profiling in HCMV-infected cells. Using relatively conservative thresholds, we identified 21 viral transcripts that contain enriched m^6A peaks that were specific to wild-type but not to METTL3-depleted cells (Supplementary Table 2). To investigate the effects of m^6A modification on viral gene expression, we conducted RNA-seq on METTL3-depleted and control cells 28 hpi with HCMV. This relatively early time point was chosen to allow capturing direct effects of m^6A modification. Although we observed subtle but significant reduction in the overall viral gene expression in METTL3-depleted cells (Fig. 2a), we did not detect significant changes in the expression of viral transcripts that were found to be m^6A-modified (Fig. 2b). In contrast, when we examined differences in cellular gene expression we discovered a modular and specific induction of interferon-stimulated genes (ISGs) upon METTL3 depletion (Fig. 2c). These results suggested that the inhibition in viral growth might not stem from m^6A-mediated regulation of viral gene expression but rather from m^6A-mediated regulation of the type I IFN response.

To confirm that the observed inhibition in viral growth in the absence of m^6A is indeed due to more potent IFN response, we tested whether inhibition of IFN signaling affects HCMV propagation in cells depleted of m^6A machinery proteins. To this end we used Ruxolitinib, a potent and selective Janus kinase (JAK) 1 and 2 inhibitor[37] that blocks the signaling downstream of the type I IFN receptors. In agreement with our expression measurements, HCMV propagation in cells depleted of either METTL3 or YTHDF2 were rescued by Ruxolitinib treatment, whereas propagation in control cells was impacted to a reduced extent (Fig. 2d). We further confirmed that Ruxolitinib treatment abolished the differences in ISG expression between METTL3-depleted and control cells (Supplementary Fig. 2a). The rescue in viral growth when IFN signaling is blocked illustrates that the main mechanism underlying HCMV inhibition in cells depleted of the m^6A pathway proteins involves an enhanced IFN response.

The elevated ISG expression in METTL3-depleted cells is independent of viral gene expression

We considered three possibilities for how depletion of m^{6}A 'writers' or 'readers' results in an enhanced IFN response. Since it was suggested that m^{6}A modification may diminish recognition of viral RNAs by cellular immune sensors such as Toll-like receptor 3 (TLR3) and RIG-I[38,39], we first considered the possibility that the absence of m^{6}A residues on viral transcripts is sensed as "non-self" by host sensors, triggering stronger innate immune response. To test this possibility, we infected METTL3-depleted and control cells with a UV-inactivated virus (from which no viral genes can be transcribed), and conducted RNA-seq at 22 hpi. Although after UV inactivation no viral transcripts were expressed, we still observed significant increased induction of ISG expression in METTL3-depleted cells (Fig. 3a,b), demonstrating that the elevation in ISG expression was independent of viral RNA expression. Furthermore, when METTL3-depleted and control cells were infected with HCMV for 5 h, we observed high but similar ISG expression in control and METTL3-depleted cells (Fig. 3a,c), indicating that the differences in ISG expression occurs only at later stages of infection and are therefore probably not related to differences in host recognition which takes place at the first hours post infection. These results support a direct effect of m^{6}A modification on the IFN pathway.

ISGs are not directly regulated by m^{6}A modification

Since m^{6}A was shown to promote destabilization of transcripts and was suggested to act on groups of co-regulated transcripts[11], we next considered a second possibility, namely that ISG mRNA stability is directly regulated by m^{6}A, resulting in greater abundance of ISG mRNAs in cells depleted of m^{6}A 'writers' or 'readers'. Mapping cellular transcripts that were m^{6}A-modified in HCMV-infected cells (Supplementary Table 3) revealed that ISGs were not enriched in m^{6}A peaks (Fig. 3d). Furthermore, we measured RNA decay in METTL3-depleted and control cells infected with HCMV and found no differences in the decay rates of ISGs (Fig. 3e,f and Supplementary Fig. 2b-e). These results led us to conclude that the increased ISG expression in cells lacking m^{6}A is probably related to their enhanced transcription and not to changes in their decay rates.

IFNB mRNA is m^{6}A-modified and is more stable in METTL3- and YTHDF2-depleted cells

We thus considered a third possibility, namely that the induction of ISGs upon METTL3 depletion was a consequence of stabilization of a common signaling component upstream of them, mediated by the absence of m^{6}A. The IFN response is initiated by recognition of pathogen-associated molecular patterns (PAMPs) by cellular sensors. These sensors trigger signaling cascades resulting in phosphorylation of the transcription factors IRF3 and IRF7 that leads to transcription and secretion of type I IFNs, namely IFN-α and IFN-β. Subsequently, type I IFNs bind to the interferon receptor and activate the Janus kinase (JAK) - signal transducer and activator of transcription (STAT) pathway, leading to transcription of hundreds of ISGs[40]. Consistent with our hypothesis, at 24 hpi STAT1 phosphorylation was increased in METTL3-depleted cells compared to control cells (Fig. 4a and Supplementary Fig. 2f). Conversely, we did not observe substantial differences in the amount of IRF3 and IRF7 phosphorylation (Fig. 4a), indicating that the enhanced expression of ISGs is mostly independent of differences in PAMP recognition by cellular sensors. The absence of differences in IRF3 and IRF7 phosphorylation, as compared to differences observed in STAT1 phosphorylation, pointed to the possibility that differential ISG expression was related to differences in the abundance of type I IFNs which are induced by IRFs and signal via JAK-STAT pathway. Since the main type I IFN that is expressed by human non-immune cells is IFN-β, we examined whether *IFNB* mRNA is modified by m^{6}A. Genome-wide mapping of m^{6}A methylation at 6 hpi, when *IFNB* mRNA is still highly expressed, revealed that *IFNB* mRNA exhibited prominent m^{6}A peaks in the vicinity of its stop codon (Fig. 4b). The m^{6}A signal was specific as it was reduced when METTL3 was depleted (Supplementary Fig. 3a). In agreement with the equivalent efficiencies of the initial infection and the similar expression of ISGs we observed at early time points post infection, no differences in *IFNB* transcript abundance was detected at 5 hpi and 8 hpi in cells depleted of METTL3 or YTHDF2 in comparison to control cells (Fig. 4c and Supplementary Fig. 3b). However, when infection progressed and *IFNB* mRNA began to decline in control cells, *IFNB* transcript abundance was significantly higher in METTL3- and YTHDF2-depleted cells (Fig. 4c and Supplementary Fig. 3b). The differences in IFN-β abundance were further validated by ELISA, demonstrating that IFN-β protein concentrations were higher at 24 hpi in METTL3-

and YTHDF2-depleted cells (Fig. 4d and Supplementary Fig. 3c). Since we observed no significant differences in *IFNB* and ISG mRNA abundance early in infection when these genes were induced, and since m^{6}A methylation was demonstrated to reduce RNA stability[3,4,7,18], we hypothesized that m^{6}A may directly regulate *IFNB* mRNA stability. To test this possibility, we performed an RNA decay assay and found that *IFNB* mRNA stability was increased in cells depleted of METTL3 and YTHDF2 as compared to control cells, whereas *USP42* mRNA that served as control transcript showed no differences in stability (Fig. 4e and Supplementary Fig. 3d).

To directly test the role of the methylated adenosines we identified by m^{6}A-immunoprecipitation in the regulation of *IFNB* stability, we ectopically expressed either a wild-type *IFNB* or *IFNB* in which the three putative m^{6}A-modified adenosines were mutated to guanosines (Supplementary Fig. 3e). Consistent with a role of these adenosines in the regulation of *IFNB* mRNA stability, although both constructs were expressed under the same promoter, the abundance of the mutant *IFNB* transcripts was two-fold higher than the wild-type *IFNB* (Fig. 4f). We further measured the stability of these transcripts and found that mutant *IFNB* mRNA was significantly more stable than the wild-type *IFNB* transcripts (Fig. 4g), indicating that these three adenosines are indeed important for regulating *IFNB* mRNA stability. Taken together, these results demonstrate that following infection, loss of m^{6}A modification leads to increased stability of *IFNB* mRNA and sustained IFN-β production, thus facilitating a stronger antiviral response that blocks HCMV propagation.

We next tested if *IFNA,* the second cytokine that participate in type I IFN response, is also regulated by m^{6}A. Since *IFNA* is mainly expressed by immune cells we used differentiated monocytic cell line, THP1. Depletion of METTL3 in THP1 cells (Supplementary Fig. 3f,g) resulted in increased expression of both *IFNA* and *IFNB* following HCMV infection, compared to control cells (Fig. 4h). These results illustrate that *IFNA* expression is also likely regulated by m^{6}A machinery.

Depletion of m^{6}A machinery led to elevated type I IFN response upon infection with diverse viruses

Since type I IFN response and ISG expression block the propagation of diverse viruses[41], we next examined whether the mechanism identified here, of m^{6}A-mediated

destabilization of *IFNB*, could serve as a mechanism affecting the propagation of additional viruses. Indeed, we found that depletion of METTL3 or YTHDF2 in Influenza A Virus (IAV)-, Adenovirus- and Vesicular Stomatitis Virus (VSV)-infected cells was accompanied by increased *IFNB* and *ISG15* expression (Fig. 5a-d). We further observed that depletion of METTL3 inhibits IAV and Adenovirus gene expression (Fig. 5e), the former in agreement with previous findings[25]. Importantly, inhibition of IFN signaling by Ruxolitinib treatment partially rescued IAV and Adenovirus gene expression in METTL3-depleted cells (Fig. 5e), demonstrating that at least part of the inhibition in viral gene expression stems from enhanced IFN response in m^{6}A-depleted cells.

Type I IFN regulation by m^{6}A methylation is conserved in mouse

Finally, we tested whether regulation of *IFNB* by m^{6}A methylation is also conserved in mouse. We re-analyzed m^{6}A maps obtained in a time-course following stimulation of mouse dendritic cells with lipopolysaccharide[42]. We found that the murine *Ifnb* mRNA was also modified by m^{6}A in vicinity to its stop codon (Fig. 6a). Importantly, out of the 14 *Ifna* isotypes, we detected expression of *Ifna*9 and *Ifna*14, both of which were m^{6}A-modified in vicinity to their stop codon (Fig. 6b and Supplementary Fig. 4a). Using CRISPR/Cas9 we generated mouse embryonic fibroblasts (MEFs) that were depleted of METTL3 or the m^{6}A 'reader' proteins YTHDF 1, 2 and 3 (Supplementary Fig. 4b,c). In agreement with our findings in human cells, infection of MEFs lacking METTL3 or YTHDF1-3 with murine CMV (MCMV) resulted in enhanced *Ifnb* and ISG expression (Fig. 6c,d). The differences in IFN-β abundance were further validated by ELISA, confirming that IFN-β protein concentrations were higher at 24 hpi in METTL3-depleted MEFs (Fig. 6e). Since non-immune murine cells express both IFN-α and IFN-β, we also tested the expression of *Ifna* and found that depletion of METTL3 or YTHDF1-3 resulted in enhanced *Ifna* expression (Fig. 6f). We next performed an RNA decay assay demonstrating that *Ifna* and *Ifnb* mRNA stability is increased in MEFs depleted of METTL3 compared to control cells, whereas a control mRNA, *Usp42* showed no differences in stability (Fig. 6g). These results illustrate that in both human and mouse cells, inhibition of m^{6}A machinery is accompanied by increased abundance of type I IFNs and ISGs after infection.

To test whether type I IFN regulation by m^{6}A also plays a role for the IFN response *in vivo*, we constructed a *Ythdf3*-deficient mouse (Supplementary Fig. 5a). *Ythdf3* deletion was validated by sequencing (Supplementary Fig. 5a) and immunoblot analysis of MEFs from *Ythdf3*$^{-/-}$ embryos (Supplementary Fig. 5b). We infected wild-type and *Ythdf3*$^{-/-}$ mice with MCMV and at 48 hpi we examined *Ifnb* and *Ifna* expression. In agreement with our *in vitro* findings, we observed significant increase in *Ifnb* and *Ifna* expression in *Ythdf3*$^{-/-}$ mice compared to wild-type controls (Fig. 6h,i), implicating the potential role of m^{6}A methylation in regulating type I IFN abundance *in vivo*.

DISCUSSION

Immunity to viral infection is characterized by the production of type I IFNs, which induce autocrine and paracrine antiviral resistance state. In resemblance to most cytokines, the type I IFN response is fine-tuned by opposing augmenting and suppressive signals; these signals are responsible to induce a rapid and effective antiviral response while restraining the magnitude and length of the response to avoid attendant toxicity. Several regulatory mechanisms that suppress type I IFN-mediated response have been characterized, including downregulation of cell surface IFNα/β receptor[43], induction of negative regulators (such as suppressor of cytokine signaling (SOCS) proteins and ubiquitin carboxyl-terminal hydrolase 18 (USP18))[44,45], and the induction of miRNAs[46].

Here we have revealed an additional, evolutionarily conserved strategy, to regulate type I IFN response, whereby m^{6}A targets *IFNB* mRNA, enhancing its destabilization and providing a novel mechanism for restricting the duration of the antiviral response. In murine cells, which express both IFN-β and IFN-α, we showed that *Ifna* is also m^{6}A-modified next to its stop codon and that depletion of the m^{6}A machinery in both mouse and human cells leads to elevation in *IFNA* abundance. These results strongly suggest that the regulatory mechanism we identified is conserved between *IFNB* and *IFNA*.

We demonstrate that upon viral infection, depletion of m^{6}A 'writer', METTL3 or the cytoplasmic m^{6}A 'reader', YTHDF2, lead to elevated levels of type I IFNs and consequently to a stronger induction of ISGs. Several observations support our conclusion that this effect is directly mediated by m^{6}A modification of IFN transcripts that regulates their decay rates.

First, we demonstrated that depletion of both METTL3 or YTHDF2 leads to specific elevation in the stability of *IFNB* transcript. Second, by ectopically expressing *IFNB*, we show that the m^6A-modified adenosines located in the proximity of *IFNB* stop codon are important for regulating *IFNB* mRNA stability. Finally, by both RNA-seq and real-time PCR, we observed no significant differences in *IFNB* and ISG mRNA abundance early in infection, when these genes are induced, but significant differences are seen at later time points post infection when IFN levels start to decline. This kinetics further supports the notion that the differences in IFN and ISG levels are mediated by differences in IFN decay rates. However, these observations do not preclude the possibility that other mechanisms, beyond elevation in IFN mRNA stability, may contribute to the stronger elevated IFN response upon depletion of m^6A machinery.

Since type I IFN affects the propagation of most viruses, our results suggest a potential unifying model for interpreting some of the diverse viral phenotypes that have been previously observed upon depletion of m^6A machinery. It is likely that for different viruses, the contribution of the mechanism we identified to the phenotypes observed upon depletion of m^6A machinery may vary. This variation will depend on the levels of type I IFN induction, the sensitivity of a given virus to type I IFN and the contribution of direct effects of m^6A modification on viral mRNA processing.

Interestingly, it has been demonstrated that pathogens exploit some of the cellular IFN negative regulatory mechanisms to escape immune responses[47]. The strong induction of m^6A machinery following HCMV infection implies that HCMV may be using this mechanism as an additional way to efficiently shut-off and escape the type I IFN response.

A recent study demonstrated that the RNA helicase DDX46 inhibits antiviral innate responses by erasing m^6A from several transcripts encoding for signaling molecules involved in the activation of type I IFN (through specific recruitment of m^6A demethylase, ALKBH5). This demethylation was suggested to enforce these transcripts retention in the nucleus and therefore to inhibit IFN production[48]. Our results imply that depletion of m^6A modification leads to prolonged expression of IFN-β and to elevation in ISG expression. Future work will have to delineate how these two, seemingly opposing mechanisms, act together.

The cytoplasmic m^{6}A 'readers', YTHDF1-3, were suggested to mediate different functions. YTHDF2 was shown to regulate instability of m^{6}A-containing mRNAs[4], whereas YTHDF1 was suggested to promote translation[5] and YTHDF3 has been proposed to serve as a co-factor to potentiate the effects of both YTHDF1 and 2[49,50]. In similarity to other studies that examined the effects of YTHDF 'readers' on viruses[26,28,29,32], depletion of YTHDF 'readers' in our experiments presented comparable effects on CMV propagation and resulted in an increase of *Ifnb* mRNA abundance. These results support the recent view that the YTHDF proteins may, under certain circumstances, promote similar functions[8].

Our results also demonstrate how rapid m^{6}A-mediated turnover of a specific mRNA can affect critical responses to external stimuli and help to maintain homeostasis. In this sense, our study provides a rationalization of how relatively subtle destabilization of an mRNA, caused by m^{6}A, can lead to strong phenotypes. While it is probable that for the majority of genes, subtle destabilization is unlikely to play a major regulatory role, in the context of tightly regulated cytokines whose expression is regulated by several feedback loops, such regulation can result in profound effect on cell physiology.

In summary, we uncover a significant and central role for m^{6}A modification in regulating innate immune homeostasis. Our findings suggest that development of m^{6}A-modulating agents may lead to novel therapeutic approaches to a range of infectious and potentially also inflammatory diseases.

ACCESSION CODES

All RNA-seq data sets generated in this manuscript have been deposited in the GEO under accession number GSE114019. Full images of immunoblots presented in this study have been deposited to Mendeley Data and are available at https://dx.doi.org/10.17632/3zb63b6ssj.1.

ACKNOWLEDGEMENTS

We thank M. Schwartz and the rest of the Stern-Ginossar lab members for discussions and critical reading of the manuscript. This research was supported by the European Research Council starting grant (StG-2014-638142), the EU-FP7-PEOPLE Career integration grant, the ICORE (Chromatin and RNA Gene Regulation) and the Israeli Science Foundation (1073/14). N.S.-G. is incumbent of the Skirball career development chair in new scientists.

AUTHOR CONTRIBUTIONS

R.W., E.G., L.L., J.H.H., S.S. and N.S.-G. conceived experiments and interpreted data. L.L., S.G. and J.H.H. generated and characterized the gene-deficient mice. R.W., E.G., M.S., S.G., C.S., A.N., J.T.-S., N.F. and M.M. executed experiments and analysis. V.T.K.L.-T. and M.T. provided critical reagents and advice. R.W., E.G. and N.S.-G. wrote the manuscript with contribution from all other authors.

COMPETING INTERESTS

The authors declare no competing interests.

REFERENCES

1. Dominissini, D. *et al.* Topology of the human and mouse m6A RNA methylomes revealed by m6A-seq. *Nature* **485,** 201–206 (2012).
2. Meyer, K. D. *et al.* Comprehensive Analysis of mRNA Methylation Reveals Enrichment in 3′ UTRs and near Stop Codons. *Cell* **149,** 1635–1646 (2012).
3. Ke, S. *et al.* m^6A mRNA modifications are deposited in nascent pre-mRNA and are not required for splicing but do specify cytoplasmic turnover. *Genes Dev.* **31,** 990–1006 (2017).
4. Wang, X. *et al.* N6-methyladenosine-dependent regulation of messenger RNA stability. *Nature* **505,** 117–120 (2014).
5. Wang, X. *et al.* N(6)-methyladenosine Modulates Messenger RNA Translation Efficiency. *Cell* **161,** 1388–1399 (2015).
6. Xiao, W. *et al.* Nuclear m6A Reader YTHDC1 Regulates mRNA Splicing. *Mol. Cell* **61,** 507–519 (2016).
7. Du, H. *et al.* YTHDF2 destabilizes m6A-containing RNA through direct recruitment of the CCR4–NOT deadenylase complex. *Nat. Commun.* **7,** 12626 (2016).
8. Meyer, K. D. & Jaffrey, S. R. Rethinking m^6A Readers, Writers, and Erasers. *Annu. Rev. Cell Dev. Biol.* **33,** 319–342 (2017).
9. Liu, J. *et al.* A METTL3–METTL14 complex mediates mammalian nuclear RNA N6-adenosine methylation. *Nat. Chem. Biol.* **10,** 93–95 (2014).
10. Zhao, B. S., Roundtree, I. A. & He, C. Post-transcriptional gene regulation by mRNA modifications. *Nat. Rev. Mol. Cell Biol.* **18,** 31–42 (2017).
11. Roundtree, I. A., Evans, M. E., Pan, T. & He, C. Dynamic RNA Modifications in Gene Expression Regulation. *Cell* **169,** 1187–1200 (2017).
12. Jia, G. *et al.* N6-methyladenosine in nuclear RNA is a major substrate of the obesity-associated FTO. *Nat. Chem. Biol.* **7,** 885–887 (2011).
13. Mauer, J. *et al.* Reversible methylation of m6Am in the 5’ cap controls mRNA stability. *Nature* **541,** 371–375 (2017).
14. Zheng, G. *et al.* ALKBH5 Is a Mammalian RNA Demethylase that Impacts RNA Metabolism and Mouse Fertility. *Mol. Cell* **49,** 18–29 (2013).
15. Schwartz, S. *et al.* High-Resolution Mapping Reveals a Conserved, Widespread, Dynamic mRNA Methylation Program in Yeast Meiosis. *Cell* **155,** 1409–1421 (2013).
16. Fustin, J.-M. *et al.* RNA-Methylation-Dependent RNA Processing Controls the Speed of the Circadian Clock. *Cell* **155,** 793–806 (2013).
17. Xiang, Y. *et al.* RNA m6A methylation regulates the ultraviolet-induced DNA damage response. *Nature* **543,** 573–576 (2017).
18. Geula, S. *et al.* Stem cells. m6A mRNA methylation facilitates resolution of naïve pluripotency toward differentiation. *Science* **347,** 1002–1006 (2015).
19. Lence, T. *et al.* m6A modulates neuronal functions and sex determination in Drosophila. *Nature* **540,** 242–247 (2016).
20. Zhang, C. *et al.* m6A modulates haematopoietic stem and progenitor cell specification. *Nature* **549,** 273–276 (2017).
21. Yoon, K.-J. *et al.* Temporal Control of Mammalian Cortical Neurogenesis by m6A Methylation. *Cell* **171,** 877–889.e17 (2017).
22. Li, H.-B. *et al.* m6A mRNA methylation controls T cell homeostasis by targeting the IL-

7/STAT5/SOCS pathways. *Nature* **548,** 338–342 (2017).
23. Tong, J. *et al.* m6A mRNA methylation sustains Treg suppressive functions. *Cell Res.* **28,** 253–256 (2018).
24. Kennedy, E. M., Courtney, D. G., Tsai, K. & Cullen, B. R. Viral Epitranscriptomics. *J. Virol.* **91,** e02263-16 (2017).
25. Courtney, D. G. *et al.* Epitranscriptomic Enhancement of Influenza A Virus Gene Expression and Replication. *Cell Host Microbe* **22,** 377–386.e5 (2017).
26. Gokhale, N. S. *et al.* N6 -Methyladenosine in Flaviviridae Viral RNA Genomes Regulates Infection. *Cell Host Microbe* **20,** 654–665 (2016).
27. Hesser, C., Karijolich, J., Dominissini, D., He, C. & Glaunsinger, B. A. N6-methyladenosine modification and the YTHDF2 reader protein play cell type specific roles in lytic viral gene expression during Kaposi's sarcoma-associated herpesvirus infection. *PLOS Pathog.* **14,** e1006995 (2018).
28. Kennedy, E. M. *et al.* Posttranscriptional m(6)A Editing of HIV-1 mRNAs Enhances Viral Gene Expression. *Cell Host Microbe* **19,** 675–685 (2016).
29. Lichinchi, G. *et al.* Dynamics of Human and Viral RNA Methylation during Zika Virus Infection. *Cell Host Microbe* **20,** 666–673 (2016).
30. Lichinchi, G. *et al.* Dynamics of the human and viral m6A RNA methylomes during HIV-1 infection of T cells. *Nat. Microbiol.* **1,** 16011 (2016).
31. Tan, B. *et al.* Viral and cellular N6-methyladenosine and N6,2'-O-dimethyladenosine epitranscriptomes in the KSHV life cycle. *Nat. Microbiol.* **3,** 108–120 (2018).
32. Tirumuru, N. *et al.* N6-methyladenosine of HIV-1 RNA regulates viral infection and HIV-1 Gag protein expression. *Elife* **5,** e15528 (2016).
33. Tsai, K., Courtney, D. G. & Cullen, B. R. Addition of m6A to SV40 late mRNAs enhances viral structural gene expression and replication. *PLoS Pathog.* **14,** e1006919 (2018).
34. Ye, F., Chen, E. R. & Nilsen, T. W. Kaposi's Sarcoma-Associated Herpesvirus Utilizes and Manipulates RNA N^6 -Adenosine Methylation To Promote Lytic Replication. *J. Virol.* **91,** e00466-17 (2017).
35. Tirosh, O. *et al.* The Transcription and Translation Landscapes during Human Cytomegalovirus Infection Reveal Novel Host-Pathogen Interactions. *PLOS Pathog.* **11,** e1005288 (2015).
36. O'Connor, C. M., Vanicek, J. & Murphy, E. A. Host microRNA regulation of human cytomegalovirus immediate early protein translation promotes viral latency. *J. Virol.* **88,** 5524–5532 (2014).
37. Lin, Q. *et al.* Enantioselective Synthesis of Janus Kinase Inhibitor INCB018424 via an Organocatalytic Aza-Michael Reaction. *Org. Lett.* **11,** 1999–2002 (2009).
38. Karikó, K., Buckstein, M., Ni, H. & Weissman, D. Suppression of RNA Recognition by Toll-like Receptors: The Impact of Nucleoside Modification and the Evolutionary Origin of RNA. *Immunity* **23,** 165–175 (2005).
39. Durbin, A. F., Wang, C., Marcotrigiano, J. & Gehrke, L. RNAs Containing Modified Nucleotides Fail To Trigger RIG-I Conformational Changes for Innate Immune Signaling. *MBio* **7,** e00833-16 (2016).
40. Ivashkiv, L. B. & Donlin, L. T. Regulation of type I interferon responses. *Nat. Rev. Immunol.* **14,** 36–49 (2014).
41. Schoggins, J. W. & Rice, C. M. Interferon-stimulated genes and their antiviral effector

functions. *Curr. Opin. Virol.* **1,** 519–525 (2011).
42. Schwartz, S. *et al.* Perturbation of m6A writers reveals two distinct classes of mRNA methylation at internal and 5' sites. *Cell Rep.* **8,** 284–296 (2014).
43. Fuchs, S. Y. Hope and Fear for Interferon: The Receptor-Centric Outlook on the Future of Interferon Therapy. *J. Interf. Cytokine Res.* **33,** 211–225 (2013).
44. Yoshimura, A., Naka, T. & Kubo, M. SOCS proteins, cytokine signalling and immune regulation. *Nat. Rev. Immunol.* **7,** 454–465 (2007).
45. Sarasin-Filipowicz, M. *et al.* Alpha Interferon Induces Long-Lasting Refractoriness of JAK-STAT Signaling in the Mouse Liver through Induction of USP18/UBP43. *Mol. Cell. Biol.* **29,** 4841–4851 (2009).
46. Gracias, D. T. *et al.* The microRNA miR-155 controls $CD8^+$ T cell responses by regulating interferon signaling. *Nat. Immunol.* **14,** 593–602 (2013).
47. Versteeg, G. A. & García-Sastre, A. Viral tricks to grid-lock the type I interferon system. *Curr. Opin. Microbiol.* **13,** 508–516 (2010).
48. Zheng, Q., Hou, J., Zhou, Y., Li, Z. & Cao, X. The RNA helicase DDX46 inhibits innate immunity by entrapping m6A-demethylated antiviral transcripts in the nucleus. *Nat. Immunol.* **18,** 1094–1103 (2017).
49. Shi, H. *et al.* YTHDF3 facilitates translation and decay of N6-methyladenosine-modified RNA. *Cell Res.* **27,** 315–328 (2017).
50. Li, A. *et al.* Cytoplasmic m6A reader YTHDF3 promotes mRNA translation. *Cell Res.* **27,** 444–447 (2017).

Figure Legends

Figure 1:

m^6A 'writers' and 'readers' are upregulated during HCMV infection and required for viral growth

(a) Immunoblot analysis of m^6A machinery proteins along HCMV infection of human foreskin fibroblasts. Actin was used as a loading control. (b and c) Viral supernatant was collected from cells depleted of m^6A machinery proteins and control cells and transferred to recipient wild-type fibroblasts. 48 h later, the recipient cells were analyzed by flow cytometry. The values present the ratio of the percentage of GFP positive cells relative to the control, indicating viral titers (n = 2, cell culture replicates). Dots, measurements; bars, mean. *P*-value by two-sided student's t-test. (d) Immunoblot analysis of HCMV Immediate-early (IE1-pp72) protein (upper panel) and fluorescent microscopy of GFP signal (lower panel), at 24 hpi in m^6A machinery depleted cells and control cells. GAPDH was used as a loading control. (e) Immunoblot analysis of HCMV immediate early (IE1-pp72), early (UL44) and late (pp28) proteins, in METTL3-depleted and control cells, at 24, 48 and 72 hpi. GAPDH was used as a loading control. (a,d,e) Gel images were cropped to present only relevant proteins. Data are representative of two (a,d,e) or three (b,c) independent experiments.

Figure 2:

Inhibition of HCMV growth in m^6A-deficient cells is driven by enhanced type I interferon response

(a) Percentage of viral reads out of total uniquely aligned reads in METTL3-depleted and control cells, as measured by RNA-seq at 28 hpi (n = 2). Dots, measurements; bars, mean. *P*-value by likelihood ratio test. (b) Viral gene expression in METTL3-depleted versus control cells, as measured in (a). Putative m^6A-modified viral transcripts are marked in blue. (c) Volcano plot showing changes in cellular transcripts levels in METTL3-depleted cells versus control cells at 28 hpi, as measured in (a). The $\log_2$ fold change between METTL3-depleted and control cells and $-\log_{10}$ of the FDR are represented in the x and y axis, respectively. ISGs are marked in red. *P*-value by hypergeometric test. (d) Viral supernatant was collected from METTL3- and YTHDF2-depleted and control cells, treated or untreated with Ruxolitinib and transferred to recipient wild-type fibroblasts. 48 h later, the recipient cells were analyzed by flow cytometry.

The values present the ratio of percentage of GFP positive cells relative to control (n = 2, cell culture replicates). Dots, measurements; bars, mean. *P*-value by two-factor ANOVA test. Data are representative of three independent experiments.

Figure 3:

ISG enhanced expression in METTL3-depleted cells is independent of viral gene expression

(a) ISG relative expression, as measured by RNA-seq, in METTL3-depleted cells versus control cells at 22 hpi, 22 h after infection with UV-inactivated virus (22uv) and at 5 hpi. Expression levels of each transcript were normalized to a scale of 0 to 1. ISGs showing significant difference (FDR < 0.01) between control and METTL3-depleted cells at 22 hpi are presented. (b and c) Cumulative distribution of cellular transcript expression in METTL3-depleted cells versus control cells at 22 h after infection with UV-inactivated virus (b), or at 5 hpi with an active virus (c), as measured in (a). *P*-value by two-sided student's t-test. (d) Quantification of putative m^6A methylation sites on ISGs compared to all other transcripts, measured by peaks identified by RNA-seq of m^6A immuno-precipitated samples (n = 3). (e) METTL3-depleted and control cells were treated with Actinomycin D at 22 hpi and harvested for RNA-seq at 0, 2 and 4 h post treatment. The decay ratio of ISGs compared to all other transcripts is presented (n = 2 for each time point). (d,e) Thick line, median; box boundaries, 25% and 75% percentiles; whiskers, 1.5-fold interquartile range. (f) mRNA decay of *OASL* in METTL3-depleted compared to control cells, as measured in (e). Values represent the mean of RNA-seq replicates and error bars show SD.

Figure 4:

IFNB mRNA is m^6A-modified and is more stable in METTL3-depleted cells

(a) Immunoblot analysis of total and phosphorylated forms of STAT1, IRF3 and IRF7 in METTL3-depleted and control cells at 24 hpi. GAPDH was used as a loading control. Gel image was cropped to present only relevant proteins. (b) RNA-seq of input RNA and m^6A immuno-precipitated RNA from 6 hpi in replicates are presented for the *IFNB* transcript. m^6A motif sequences which correspond to IP-enriched region are marked in red. (c) *IFNB* mRNA and (d) protein levels in METTL3-depleted and control cells at indicated time points post infection, measured by qRT-PCR and ELISA, respectively. *18S* ribosomal RNA was used as a normalizing

gene in qRT-PCR. Dots, measurements; bars, mean of three technical (c) and cell culture (d) replicates; *P*-value by two-sided student's t-test. (e) Nascent RNA was labeled for 2 h with 5-Ethynyluridine (EU). EU was washed out and RNA was extracted at the indicated time points. The relative remaining EU-labeled mRNA abundance, normalized to *18S* ribosomal RNA, was analyzed by qRT-PCR for *IFNB* and *USP42* that was used as control. Values represent the mean of three technical replicates and error bars show SD. *P*-value by two-sided student's t-test. (f and g) Wild-type (WT) and mutant (MUT) *IFNB* mRNA (in which three putative m^6A-modified adenosines were mutated to guanosines) were ectopically expressed in fibroblasts. At 24 hpi, *IFNB* mRNA levels were measured by qRT-PCR (f), or cells were treated with Actinomycin D and harvested at 0, 0.5, 1 and 4 h post treatment (g). Blasticidin-resistance gene, which was expressed from the same construct, was used as a normalizing gene. *P*-value by two-sided student's t-test. (f) Dots, measurements; bars, mean of three technical replicates. (g) Values represent the mean of three technical replicates and error bars show SD. (h) mRNA levels of *IFNA* and *IFNB* in HCMV-infected differentiated THP1 cells were measured by qRT-PCR at 24 hpi. *18S* ribosomal RNA was used as a normalizing gene. Dots, measurements; bars, mean of three technical replicates. *P*-value by two-sided student's t-test. Data are representative of two (a,d) or three (c,e-h) independent experiments.

Figure 5:

Depletion of m^6A machinery proteins leads to elevation in *IFNB* levels upon infection with diverse viruses

(a-d) mRNA levels of *IFNB* and *ISG15* in Influezna A-, Adenovirus- and VSV-infected METTL3-depleted (a-b) and YTHDF2-depleted (c-d) compared to control cells, were measured by qRT-PCR at 24 hpi. *18S* ribosomal RNA was used as a normalizing gene. (e) qRT-PCR analysis of Influenza *M2* and Adenovirus *L3* expression in METTL3-depleted cells and control cells (48 hpi), treated or untreated with Ruxolitinib. *18S* ribosomal RNA was used as a normalizing gene. (a-e) Dots, measurements; bars, mean of three technical replicates; *P*-value by two-sided student's t-test (a-d) and by two-factor ANOVA test (e). Data (a-e) are representative of three independent experiments.

Figure 6:

Type I IFN m^{6}A methylation and destabilization are conserved in mouse

(a and b) RNA-seq of input RNA and m^{6}A immuno-precipitated RNA from mouse dendritic cells treated with lipopolysaccharide (LPS) for 3 and 6 h is presented for *Ifnb* (a) and *Ifna9* (b). m^{6}A motif sequences which correspond to IP-enriched region are marked in red. (c and d) MEFs depleted of m^{6}A 'readers' and 'writer' proteins were infected with MCMV and harvested at 24 hpi. mRNA levels of mouse *Ifnb* (c) and *Isg15* (d) were measured by qRT-PCR. *Gapdh* was used as a normalizing gene. (e) IFN-β protein levels in METTL3-depleted and control MEFs were measured by ELISA. (f) MEFs depleted of m^{6}A 'readers' and 'writer' proteins were infected with MCMV and harvested at 12 hpi. mRNA levels of mouse *Ifna* were measured by qRT-PCR. *Gapdh* was used as a normalizing gene. (c-f) Dots, measurements; bars, mean of three technical (c,d,f) or cell culture (e) replicates; *P*-value by two-sided student's t-test. (g) Nascent RNA was labeled for 2 h with 5-Ethynyluridine (EU). EU was washed out and RNA was extracted at the indicated time points. The relative remaining EU-labeled mRNA abundance, normalized to *18S* ribosomal RNA, was analyzed by qRT-PCR for *Ifnb*, *Ifna* and *Usp42* (control). Values represent the mean of three technical replicates and error bars show SD. *P*-value by two-sided student's t-test. (h and i) *Ythdf3*$^{+/+}$ (n=12) or *Ythdf3*$^{-/-}$ (n=13) mice were infected with MCMV. *Ifnb* (h) and *Ifna* (i) mRNA levels in spleen were measured by qRT-PCR at 48 hpi. *18S* ribosomal RNA was used as a normalizing gene. Thick line, median; box boundaries, 25% and 75% percentiles; whiskers, 1.5-fold interquartile range. *P*-value by two-sided student's t-test. Data are representative of three (c,d,f,g) or two (e) independent experiments.

Tables

Supplementary Table 1

Measurements of cells viability in control cells and cells depleted of m^{6}A machinery proteins, before and 96 h post infection with HCMV.

Supplementary Table 2

Dataset of 21 putative m^{6}A sites in HCMV transcripts.

Supplementary Table 3

Dataset of 7,093 putative m^{6}A sites in human transcripts, obtained following infection with HCMV.

Methods

Cells and viruses

Human foreskin fibroblasts (HFF) (ATCC CRL-1634) and Mouse embryonic fibroblasts (MEF) were maintained in Dulbecco Modified Eagle Medium (DMEM) with 10% fetal bovine serum, 2 mM L-glutamine, and 100 units/ml penicillin and streptomycin (Beit-Haemek). THP1 cells (ATCC TIB-202) were maintained in RPMI-1640 Medium with 10% fetal bovine serum, 2 mM L-glutamine, 100 units/ml penicillin and streptomycin, 10 mM HEPES pH7.46, 1 mM sodium pyruvate, 1500 mg/L sodium bicarbonate (Beit-Haemek) and 0.05 mM 2-mercaptoethanol. The bacterial artificial chromosome (BAC) derived strain TB40E expressing an SV40-GFP reporter protein (TB40E-GFP) was previously described[36]. Virus was propagated by electroporation of infectious BAC DNA into HFF cells using the Amaxa P2 4D-Nucleofector kit (Lonza) according to the manufacturer's instructions. The human influenza virus A/Puerto Rico/8/34 H1N1 used in this study was generated as previously described[51]. The MCMV used was of strain Smith-GFP, which was previously described[52]. Adenovirus of serotype 4 was collected from patients, as previously described[53]. VSV was from ATCC (VR-1238). *In vitro* infection with Influenza virus was done at multiplicity of infection (MOI) of 0.5. All other *In vitro* infections were done at MOI of 5.

Immunoblot analysis

Cells were lysed using RIPA buffer. Lysates were centrifuged at 20,000 × *g* for 10 min at 4 °C. Samples were then separated by 4–12% polyacrylamide Bis-tris gel electrophoresis (Invitrogen), blotted onto nitrocellulose membranes and immunoblotted with primary antibodies: anti-IE1/IE2 (clone CH160, Abcam, ab53495); anti-UL44 (Virusys, CA006); anti-pp28 (Eastcoast, CA004); anti-GAPDH (Cell Signaling Technology, 2118S); anti-ACTIN (Sigma Aldrich, A4700); anti-METTL3 (Proteintech, 15073-1-AP); anti-METTL14 (Novus Biologicals, NBP1-81392); anti-YTHDF1 (Proteintech, 17479-1-AP); anti-YTHDF2 (Aviva Systems Biology, ARP67917); anti-YTHDF3 (Santa Cruz Biotechnology, SC-87503); anti-YTHDC1 (Abcam, ab122340); anti-STAT1 (Cell Signaling Technology, 14994); anti-Phosphorylated-STAT1 (Cell Signaling Technology, 9167); anti-IRF3 (Cell Signaling Technology, 4302); anti-Phosphorylated-IRF3 (Cell Signaling Technology, 4947); anti-IRF7 (Abcam, ab109255); anti-Phosphorylated-IRF7 (Cell Signaling Technology, 5184); anti-HSP90 (Epitomics, 1492-1). Secondary antibodies used

were Goat anti-rabbit, Goat anti-mouse or Goat anti-rat (IRDye 800CW or IRDye 680RD, Li-Cor). Reactive bands were detected by Odyssey CLx infrared imaging system (Li-Cor).

RT-PCR

Total RNA was extracted using Tri-Reagent (Sigma) according to manufacturer's protocol. RNA was then treated with DNaseI, using PerfeCTa DNaseI kit (Quantabio) and cDNA was prepared using qScript cDNA Synthesis Kit (Quantabio).

Real-time PCR was performed using the SYBR Green PCR master-mix (ABI) on a QuantStudio 12K Flex Real-Time PCR System (life technologies) with the following primers (forward, reverse):

Human IFNB; (5′-ACTGCAACCTTTCGAAGCCT-3′, 5′-AGCCTCCCATTCAATTGCCA-3′)

Human *IFNA*; (5′-ATTTCTGCTCTGACAACCTC-3′, 5′-CTGAATGACTTGGAAGCCTG-3′)

Human *ISG15*; (5′-TTTGCCAGTACAGGAGCTTG-3′, 5′-TTCAGCTCTGACACCGACAT-3′)

Human *GAPDH*; (5′-TGGTATCGTGGAAGGACTCA-3′, 5′-CCAGTAGAGGCAGGGATGAT-3′)

Human *18S*; (5′-GTAACCCGTTGAACCCCATT-3′, 5′-CCATCCAATCGGTAGTAGCG-3′)

Human *USP42*; (5′-ATGGCCAGGGTGATTGAAAAC-3′, 5′-CACCACGCAGATTGGAACAG-3′)

Blasticidin resistance gene; (5′-AACGGCTACAATCAACAGCA-3′, 5′-CGATCGCGACGATACAAGTC-3′)

Mouse *Ifnb*; (5′-AACCTCACCTACAGGGCGGACTTCA-3′, 5′-TCCCACGTCAATCTTTCCTCTTGCTTT-3′)

Mouse *Ifna*; (5′-GGACTTTGGATTCCCGCAGGAGAAG-3′, 5′-GCTGCATCAGACAGCCTTGCAGGTC-3′)

Mouse *Isg15*; (5′-TCTGACTGTGAGAGCAAGCAG-3′, 5′-ACCTTTAGGTCCCAGGCCATT-3′)

Mouse *Gapdh*; (5′-TCAAGCTCATTTCCTGGTATGACA-3′, 5′-TAGGGCCTCTCTTGCTCAGT-3′)

Mouse *Usp42*; (5′-TCTTCCTGGAAAGGTGACGC-3′, 5′-CTTTGGAGAGCTTCCCCCTG-3′)

Influenza *M2*; (5′-CGAGGTCGAAACGCCTATCA-3′, 5′-GAAGGCCCTCCTTTCAGTCC-3′)

Adenovirus *L3*; (5′-GGCACGGGACTCCGCGCAAGGAC-3′, 5′-

CTTAAGCCCGCTCCAGAGAC-3′)

Plasmids and sgRNAs

All gene silencing was done using CRISPR/Cas9 system, with lentiCRISPR v2 plasmid (Addgene#52961)[54]. The following sgRNAs were cloned downstream of U6 promoter:

Human & mouse *METTL3*: 5′-GGACACGTGGAGCTCTATCC-3′

Human *METTL14*: 5′-GCCGTAACTTCTGCCGCTCC-3′

Human *WTAP*: 5′-GCGGGAGGAGCTACCATTACT-3′

Human *YTHDF1*: 5′-GAATGGACGGCGGGTAATAGC-3′

Human *YTHDF2*: 5′-GATGGAGGGACTGTAGTAACT-3′

Human *YTHDF3*: 5′-GCTAAGCGAATATGCCGTAAT-3′

Human *FTO*: 5′-GCACTTCATCTTGTCCGTTGT-3′

Human *ALKBH5*: 5′-GCCTCATAGTCGCTGCGCTCG-3′

Human *IGSF8* (Control): 5′-GCGGCAGCAGCGTGGGCCTGA-3′

Mouse *Igsf8* (Control): 5′-GGAGCGAACTCAGCGGCGTG-3′

Mouse *Ythdf1*: 5′-GAAGCATGTCGGCCACCAGCG-3′

Mouse *Ythdf2*: 5′-GTGAGGATCCGAGAGCCATGT-3′

Mouse *Ythdf3*: 5′-GATATATGGATCTGACATTGG-3′

Lentiviruses were generated by co-transfection of lentiCRISPR v2 constructs and 2nd generation packaging plasmids (psPAX2, Addgene#12260 & pMD2.G, Addgene#12259), using jetPEI DNA transfection reagent (Polyplus transfection) into HEK293T cells, according to manufacturer's instructions. 48 h post transfection, supernatants were collected and filtered through 0.45μm PVDF filter (Millex). To induce gene silencing in fibroblasts, cells were transduced with lentivirus expressing sgRNA and were puromycin-selected (1.75μg/mL) for 4–5 days. The depletion of target proteins was confirmed by immunoblot analysis and experiments were done within 6 days after transduction of the lentivirus.

Cells treatments and ELISA

Cells were resuspended in PBS and propidium iodide was added at concentration of 1μg/mL for 1 min prior to analysis in flow cytometer. Ruxolitinib (InvivoGen) was used at final

concentration of 4μM and added to growth media 1 h post infection (hpi). For ELISA, supernatant from METTL3- or YTHDF2-depleted and control cells was collected at 24 hpi and analyzed by Human IFN Beta ELISA Kit or Mouse Ifn Beta ELISA Kit (pbl Assay Science).

RNA decay assays

Actinomycin D (Sigma Aldrich) was used at final concentration of 5μM. At each time point, two independent wells of METTL3-depleted cells and two independent wells of control cells were harvested. To calculate RNA decay rate, first we normalized the number of reads for each transcript to follow the global degradation rate in each time point, based on median degradation level in mammalian cells. Decay rate for each transcript was calculated as the slope of linear regression of the log of the normalized number of reads as function of time.
5-Ethynyluridine (EU) labeling and pull-down was done using the Click-It Nascent RNA Capture Kit (Invitrogen).

Generation of plasmids

The plasmids containing wild-type and mutant *IFNB* were derived from the pLex_TRC206 plasmid[55]. eGFP sequence was replaced, using XmaI and BamHI sites, with *IFNB*, with or without mutations of three putative m^6A-modified adenosines.

Next-generation sequencing and data analysis

Raw sequences obtained from NextSeq500 (Illumina) were first trimmed at their 3′ end, removing the polyA tail. Alignment was performed using Bowtie (allowing up to 2 mismatches) and reads were aligned to concatenation of the human (hg19) and the viral genomes (NCBI EF999921.1). Reads aligned to ribosomal RNA were removed. Reads that were not aligned to the genome were then aligned to the transcriptome.

Statistics

Differential gene expression was calculated using edgeR with default parameters[56].
ISGs were defined as genes which were ≥4-fold induced, following a 5 h treatment with type I interferons[35]. ISG enrichment was calculated using hypergeometric test. *P*-value for reduction in

viral gene expression in METTL3-depleted cells was calculated using likelihood ratio test, with logistic regression of viral reads.

Differences in Ruxolitinib effect between control and METTL3-depleted cells or control and YTHDF2-depleted cells were calculated by two-factor ANOVA. For Fig. 2d, Degrees of freedom = 4, F = 1010.5 (METTL3), F = 498.7 (YTHDF2). For Fig. 5e, Degrees of freedom = 8, F = 1602.3 (IAV), F = 14.9 (Adenovirus).

Detection of putative m^{6}A sites

m^{6}A pull-down and preparation of RNA-seq libraries were done as previously described[15,42]. Two sets of m^{6}A-seq experiments were performed at 72 hpi and at 6 hpi. Both experiments included 3 replicates of wild-type samples and 3 replicates of METTL3-depleted samples. In both experiments, both the immuno-precipitated fraction (IP) and non-immuno-precipitated samples (Input) were sequenced. m^{6}A-seq data was aligned separately to the human and HCMV genomes using STAR aligner[57]. We then applied a previously published approach to identify putative m^{6}A sites[42], and to assign each putative site with a Peak Over Median (POM) score, capturing the fold change of enrichment in the peak region over the median coverage of the gene harboring it, and Peak Over Input (POI) score, capturing the fold change of enrichment over the corresponding region in the Input (non-enriched) control experiment. To identify sites specific to wild-type, but absent upon METTL3-depleted samples, we performed two separate T tests: The first assessed, for each putative peak, whether the distribution of POM scores in wild-type samples differed significant ($P < 0.05$) from METTL3-depleted samples; The second assessed the same for the POI scores. A site was deemed as significant if (1) both its mean POM (across the triplicates) and mean POI scores in the wild-type samples exceeded the corresponding value in the METTL3-depleted samples, and (2) if at least one of the two above calculated *P* values was significant.

Generation of *Ythdf3*$^{-/-}$ mice and infection with MCMV

T7 promoter was added to the Cas9 coding region by PCR amplification of px330 plasmid (Addgene#42230)[58], using T7-Cas9 F and Cas9 R primers. The T7-Cas9 PCR product was gel purified and used as the template for *in vitro* transcription (IVT) using mMESSAGE mMACHINE T7 ULTRA kit (Thermo Fisher Scientific). In order to generate *Ythdf3* sgRNA,

gRNA primers, g*Ythdf3* F+R, were cloned into px330 plasmid. T7 promoter was added to the gRNA template by PCR amplification of px330, using T7-sg*Ythdf3* F and sg*Ythdf3* R. The T7-sgRNA PCR product was gel purified and used as the template for IVT using MEGA shortscript T7 kit (Thermo Fisher Scientific). Both the Cas9 mRNA and the sgRNAs were purified using the MEGA clear kit (Thermo Fisher Scientific).

CB6F1 (C57BL/6 × BALB/c) and ICR mice strains were used as embryo donors and foster mothers, respectively. Superovulated CB6F1 mice (8-10 weeks old) were mated to CB6F1 stud males, and fertilized embryos were collected from oviducts. Cas9 mRNAs and sgRNA (50 ng/μl) was injected into the cytoplasm of fertilized eggs with well recognized pronuclei in M2 medium (Sigma). The injected zygotes were cultured in KSOM with amino acids (Sigma) at 37 °C under 5% CO2 in air until blastocyst stage by 3.5 days. Thereafter, 15–25 blastocysts were transferred into uterus of pseudopregnant ICR females at 2.5 d post-coitum (dpc). Mutated animals were screen for indels by sequencing with *Ythdf3* seq F+R primers. *Ythdf3*$^{+/-}$ animal were backcrossed with C57BL/6 mice for 2 generation before mating in order to generate *Ythdf3*$^{-/-}$ mice. For *in vivo* experiments mice (n = 25) were infected with 2 x 10^5 pfu by intraperitoneal injection. One *Ythdf3*$^{+/+}$ mouse was mock-infected with PBS. At 48 hpi, they were euthanized and spleens were harvested, homogenized and RNA was extracted. All animal studies were conducted according to the guidelines and following approval of the Weizmann Institute of Science (IACUC approval #33900217-2).

Primers (forward, reverse):

T7-Cas9; (5′-TAATACGACTCACTATAGGGAGAATGGACTATAAGGACCACGAC-3′, 5′-GCGAGCTCTAGGAATTCTTAC-3′)

g*Ythdf3*; (5′-CACCGTTTGTCTGGCTACTTAAGTA-3′, 5′-AAAC TACTTAAGTAGCCAGACAAAC-3′)

T7-sg*Ythdf3*; (5′-TTAATACGACTCACTATAGGTTTGTCTGGCTACTTAAGTA-3′, 5′-AAAAGCACCGACTCGGTGCC-3′)

Ythdf3 seq; (5′-CAAGGTTAGCCTGGGTTACAGAAGAAA-3′, 5′-CTAGTCATTATCCCATGAAAGTTTCCAGC-3′)

Reporting summary

Further information on research design is available in the Life Sciences Reporting Summary, which is linked to this article.

DATA AVAILABILITY

All RNA-seq data sets generated in this manuscript have been deposited in the GEO under accession number GSE114019. Full images of immunoblots presented in this study have been deposited to Mendeley Data and are available at https://dx.doi.org/10.17632/3zb63b6ssj.1. All other data are available from the corresponding author upon reasonable request.

REFERENCES

51. Achdout, H. *et al.* Enhanced recognition of human NK receptors after influenza virus infection. *J. Immunol.* **171,** 915–923 (2003).
52. Wang, X. *et al.* Murine cytomegalovirus abortively infects human dendritic cells, leading to expression and presentation of virally vectored genes. *J. Virol.* **77,** 7182–7192 (2003).
53. Meningher, T. *et al.* Relationships between A(H1N1)pdm09 influenza infection and infections with other respiratory viruses. *Influenza Other Respi. Viruses* **8,** 422–430 (2014).
54. Sanjana, N. E., Shalem, O. & Zhang, F. Improved vectors and genome-wide libraries for CRISPR screening. *Nat. Methods* **11,** 783–784 (2014).
55. Straussman, R. *et al.* Tumour micro-environment elicits innate resistance to RAF inhibitors through HGF secretion. *Nature* **487,** 500–504 (2012).
56. McCarthy, D. J., Chen, Y. & Smyth, G. K. Differential expression analysis of multifactor RNA-Seq experiments with respect to biological variation. *Nucleic Acids Res.* **40,** 4288–4297 (2012).
57. Dobin, A. *et al.* STAR: ultrafast universal RNA-seq aligner. *Bioinformatics* **29,** 15–21 (2013).
58. Cong, L. *et al.* Multiplex Genome Engineering Using CRISPR/Cas Systems. *Science* **339,** 819–823 (2013).

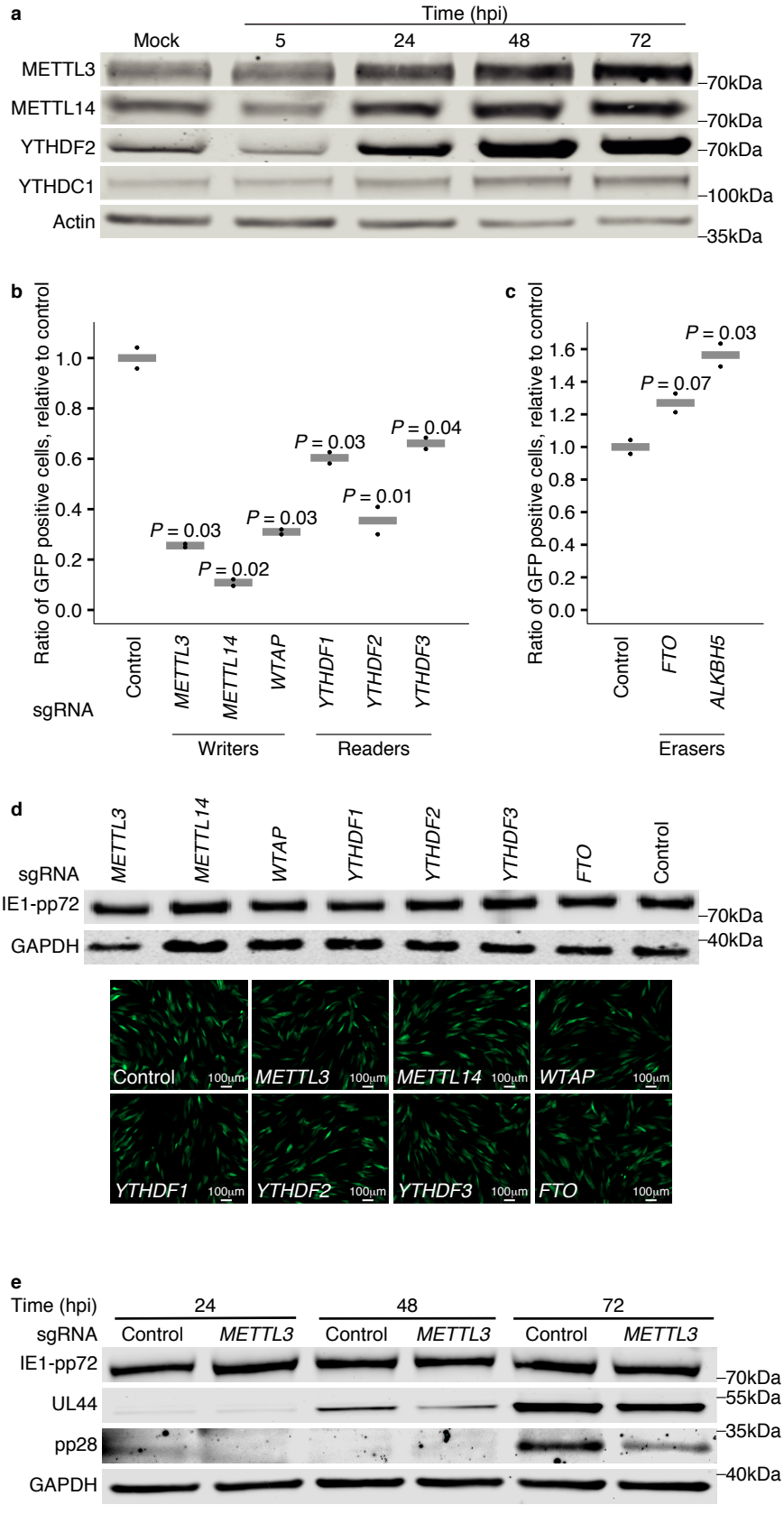
a
Time (hpi)
Mock
5
24
48
72
METTL3
METTL14
YTHDF2
YTHDC1
Actin
70kDa
70kDa
70kDa
100kDa
35kDa
b
Ratio of GFP positive cells, relative to control
P = 0.03
P = 0.02
P = 0.03
P = 0.03
P = 0.01
P = 0.04
Control
METTL3
METTL14
WTAP
YTHDF1
YTHDF2
YTHDF3
sgRNA
Writers
Readers
c
Ratio of GFP positive cells, relative to control
P = 0.07
P = 0.03
Control
FTO
ALKBH5
Erasers
d
sgRNA
METTL3
METTL14
WTAP
YTHDF1
YTHDF2
YTHDF3
FTO
Control
IE1-pp72
GAPDH
70kDa
40kDa
Control
METTL3
METTL14
WTAP
YTHDF1
YTHDF2
YTHDF3
FTO
100μm
e
Time (hpi)
24
48
72
sgRNA
Control
METTL3
Control
METTL3
Control
METTL3
IE1-pp72
UL44
pp28
GAPDH
70kDa
55kDa
35kDa
40kDa

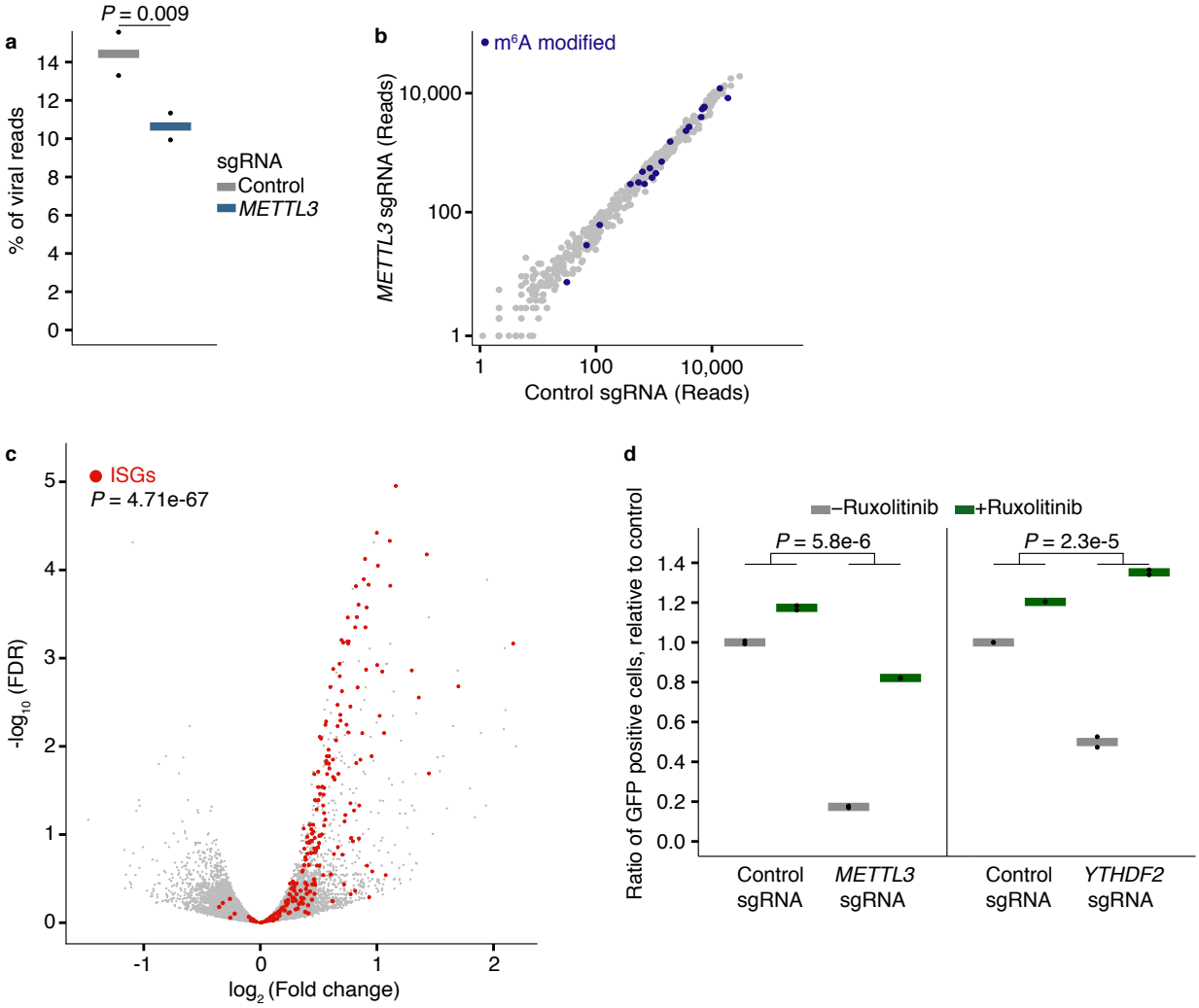
a
P = 0.009
% of viral reads
sgRNA
Control
METTL3
b
m6A modified
METTL3 sgRNA (Reads)
Control sgRNA (Reads)
c
ISGs
P = 4.71e-67
-log10 (FDR)
log2 (Fold change)
d
−Ruxolitinib
+Ruxolitinib
P = 5.8e-6
P = 2.3e-5
Ratio of GFP positive cells, relative to control
Control sgRNA
METTL3 sgRNA
Control sgRNA
YTHDF2 sgRNA

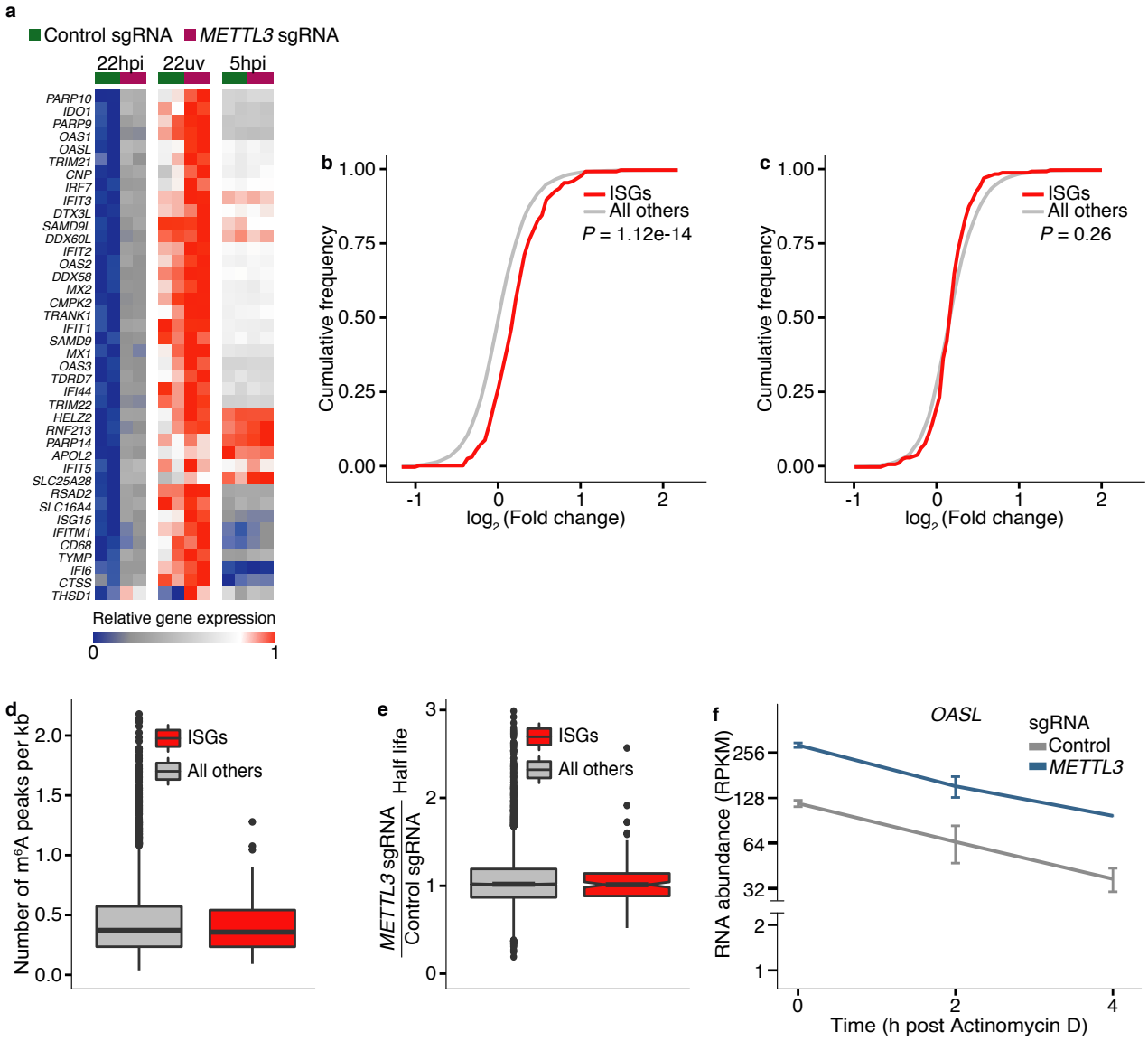
a
Control sgRNA
METTL3 sgRNA
22hpi
22uv
5hpi
PARP10
IDO1
PARP9
OAS1
OASL
TRIM21
CNP
IRF7
IFIT3
DTX3L
SAMD9L
DDX60L
IFIT2
OAS2
DDX58
MX2
CMPK2
TRANK1
IFIT1
SAMD9
MX1
OAS3
TDRD7
IFI44
TRIM22
HELZ2
RNF213
PARP14
APOL2
IFIT5
SLC25A28
RSAD2
SLC16A4
ISG15
IFITM1
CD68
TYMP
IFI6
CTSS
THSD1
Relative gene expression
0
1
b
Cumulative frequency
1.00
0.75
0.50
0.25
0.00
ISGs
All others
P = 1.12e-14
-1
0
1
2
log2 (Fold change)
c
Cumulative frequency
1.00
0.75
0.50
0.25
0.00
ISGs
All others
P = 0.26
-1
0
1
2
log2 (Fold change)
d
Number of m6A peaks per kb
2.0
1.5
1.0
0.5
0.0
ISGs
All others
e
METTL3 sgRNA / Control sgRNA Half life
3
2
1
0
ISGs
All others
f
OASL
sgRNA
Control
METTL3
RNA abundance (RPKM)
256
128
64
32
2
1
0
2
4
Time (h post Actinomycin D)

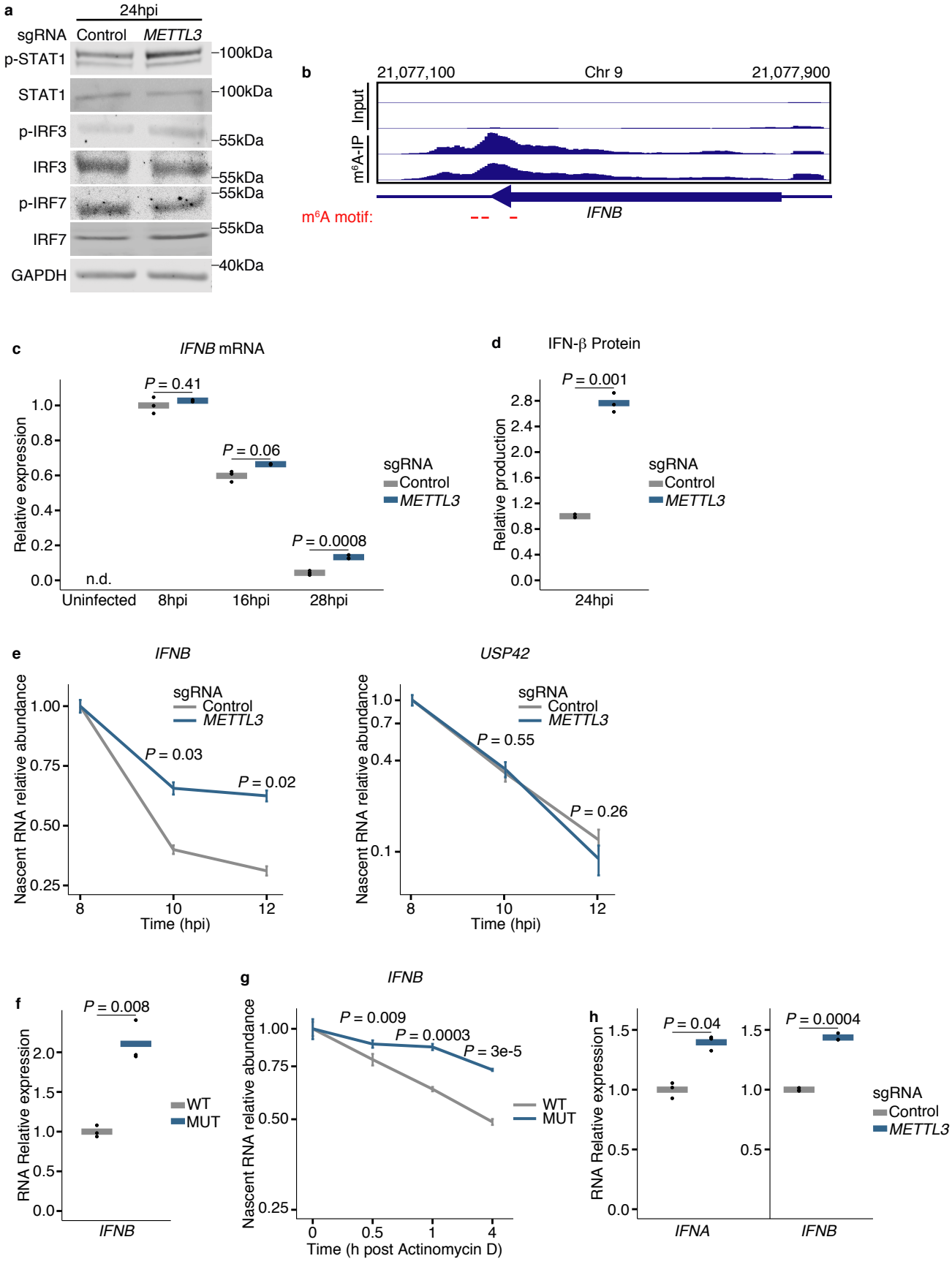
a
24hpi
sgRNA Control METTL3
p-STAT1
STAT1
p-IRF3
IRF3
p-IRF7
IRF7
GAPDH
100kDa
100kDa
55kDa
55kDa
55kDa
55kDa
40kDa
b
21,077,100
Chr 9
21,077,900
Input
m6A-IP
m6A motif:
IFNB
c
IFNB mRNA
P = 0.41
P = 0.06
P = 0.0008
n.d.
Relative expression
Uninfected
8hpi
16hpi
28hpi
sgRNA
Control
METTL3
d
IFN-β Protein
P = 0.001
Relative production
24hpi
sgRNA
Control
METTL3
e
IFNB
USP42
sgRNA
Control
METTL3
P = 0.03
P = 0.02
P = 0.55
P = 0.26
Nascent RNA relative abundance
Time (hpi)
f
P = 0.008
RNA Relative expression
WT
MUT
IFNB
g
IFNB
P = 0.009
P = 0.0003
P = 3e-5
Nascent RNA relative abundance
WT
MUT
Time (h post Actinomycin D)
h
P = 0.04
P = 0.0004
RNA Relative expression
IFNA
IFNB
sgRNA
Control
METTL3

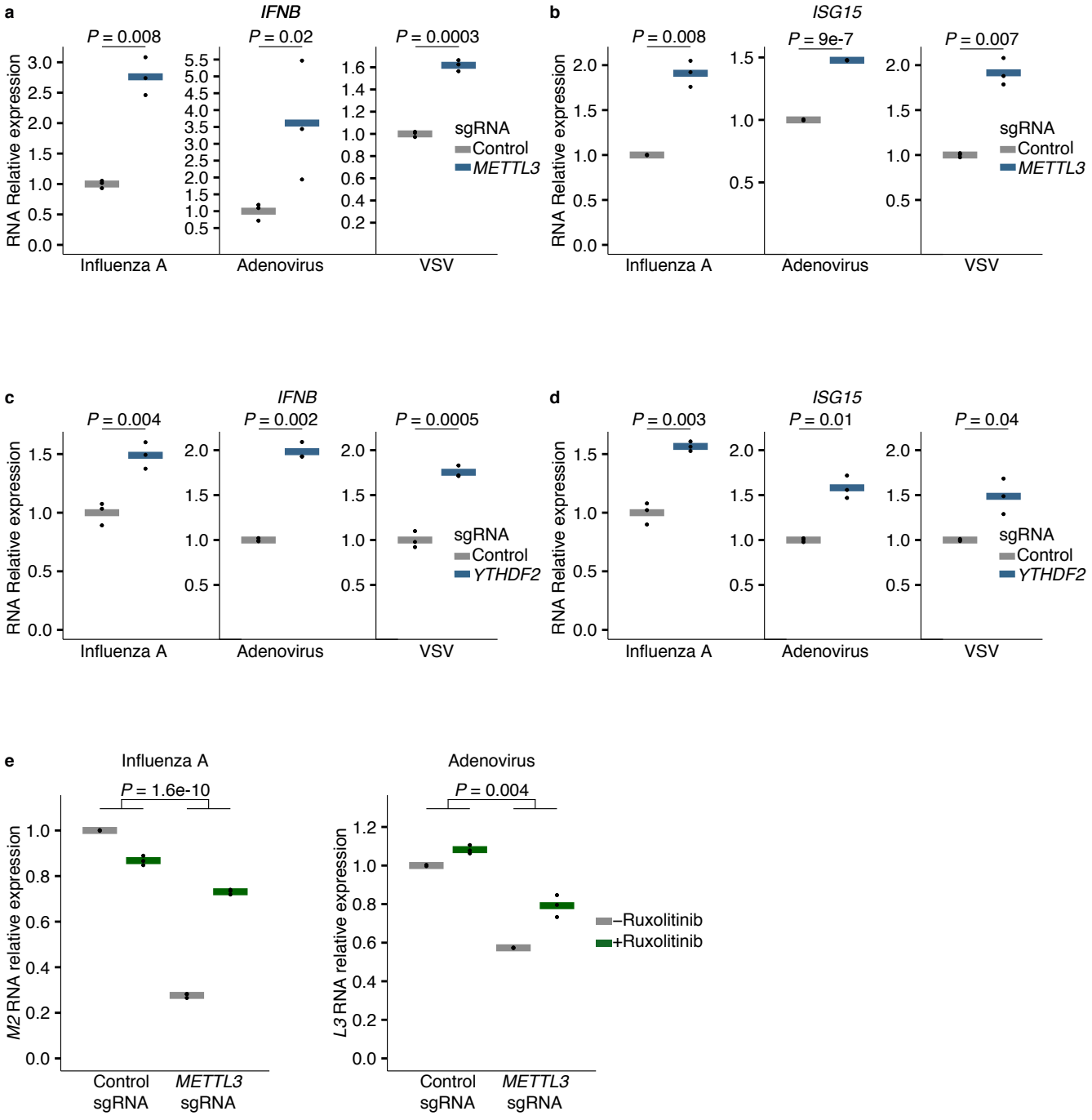
a
IFNB
P = 0.008
P = 0.02
P = 0.0003
RNA Relative expression
Influenza A
Adenovirus
VSV
sgRNA
Control
METTL3
b
ISG15
P = 0.008
P = 9e-7
P = 0.007
c
IFNB
P = 0.004
P = 0.002
P = 0.0005
YTHDF2
d
ISG15
P = 0.003
P = 0.01
P = 0.04
e
Influenza A
P = 1.6e-10
M2 RNA relative expression
Control sgRNA
METTL3 sgRNA
Adenovirus
P = 0.004
L3 RNA relative expression
–Ruxolitinib
+Ruxolitinib

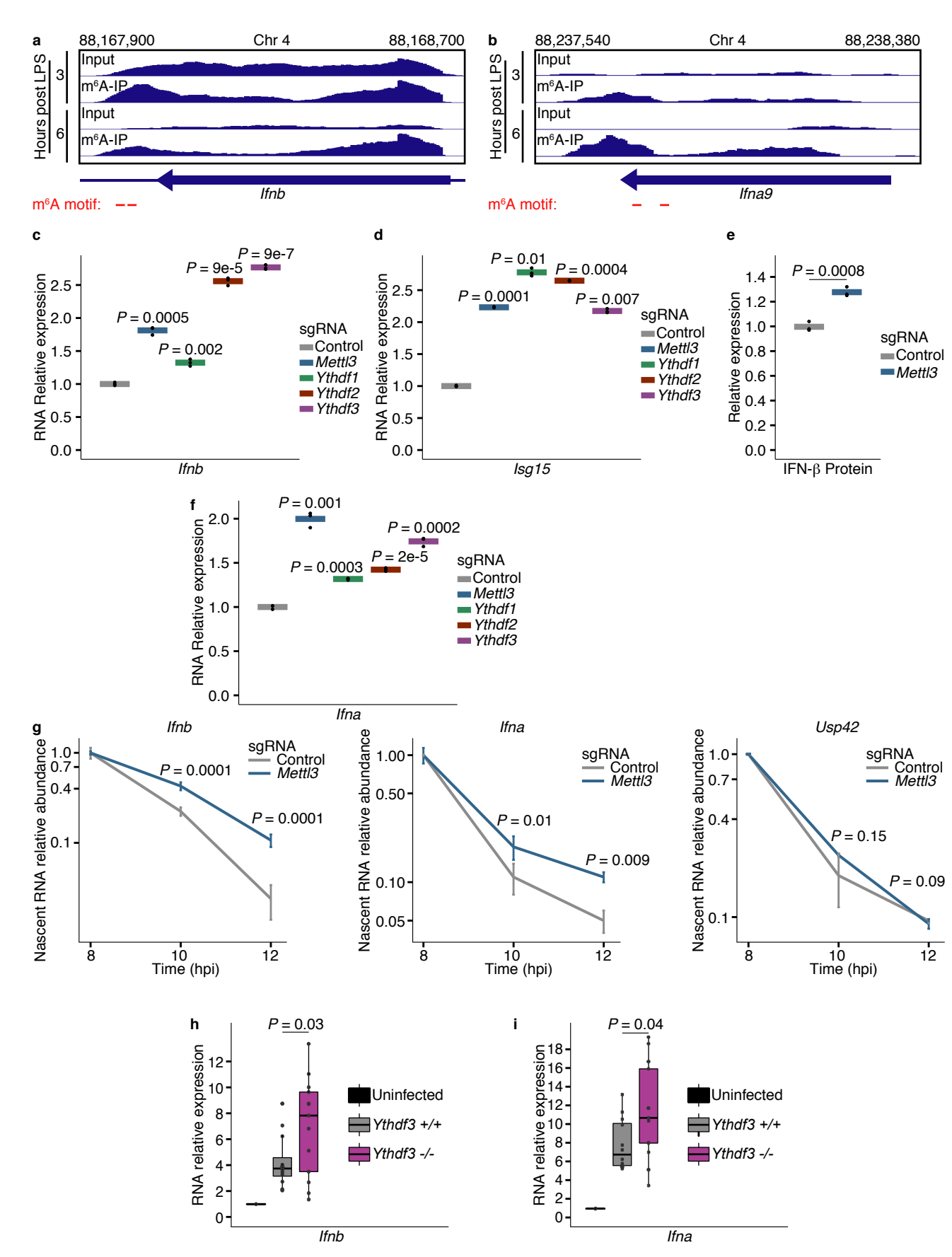
a
88,167,900
Chr 4
88,168,700
Hours post LPS
3
6
Input
m6A-IP
Input
m6A-IP
Ifnb
m6A motif:
b
88,237,540
Chr 4
88,238,380
Hours post LPS
3
6
Input
m6A-IP
Input
m6A-IP
Ifna9
m6A motif:
c
RNA Relative expression
P = 9e-7
P = 9e-5
P = 0.0005
P = 0.002
sgRNA
Control
Mettl3
Ythdf1
Ythdf2
Ythdf3
Ifnb
d
RNA Relative expression
P = 0.01
P = 0.0004
P = 0.0001
P = 0.007
sgRNA
Control
Mettl3
Ythdf1
Ythdf2
Ythdf3
Isg15
e
Relative expression
P = 0.0008
sgRNA
Control
Mettl3
IFN-β Protein
f
RNA Relative expression
P = 0.001
P = 0.0002
P = 0.0003
P = 2e-5
sgRNA
Control
Mettl3
Ythdf1
Ythdf2
Ythdf3
Ifna
g
Ifnb
Nascent RNA relative abundance
sgRNA
Control
Mettl3
P = 0.0001
P = 0.0001
Time (hpi)
Ifna
Nascent RNA relative abundance
sgRNA
Control
Mettl3
P = 0.01
P = 0.009
Time (hpi)
Usp42
Nascent RNA relative abundance
sgRNA
Control
Mettl3
P = 0.15
P = 0.09
Time (hpi)
h
RNA relative expression
P = 0.03
Uninfected
Ythdf3 +/+
Ythdf3 -/-
Ifnb
i
RNA relative expression
P = 0.04
Uninfected
Ythdf3 +/+
Ythdf3 -/-
Ifna

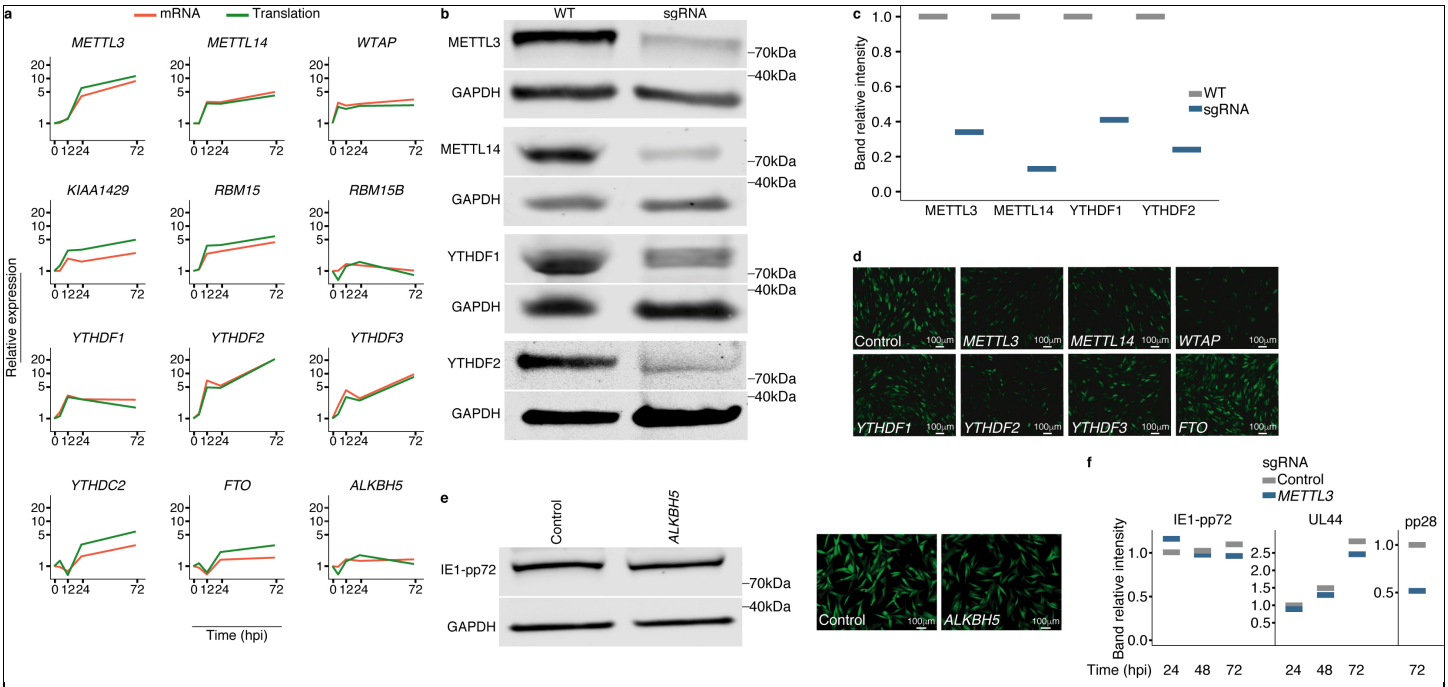

Supplementary Figure 1

m^{6}A machinery is elevated along HCMV infection and is important for its propagation

(a) mRNA and translation levels of genes encoding for m^{6}A machinery along HCMV infection, as measured by RNA-seq (red) and ribosome profiling (green)[35]. (b) Immunoblot analysis of m^{6}A machinery proteins in cells expressing sgRNAs targeting control gene (WT) or the various m^{6}A machinery genes (indicated on the left) in fibroblasts. GAPDH was used as a loading control. Gel image was cropped to present only relevant proteins. (c) Quantification of m^{6}A machinery proteins levels from the immunoblot analysis in (b) normalized to the levels of GAPDH. (d) Fluorescent microscopy of GFP signal in WT fibroblasts infected with supernatant from infected cells in which m^{6}A machinery genes were depleted (indicated at the bottom). (e) Immunoblot analysis of HCMV Immediate-early protein (IE1-pp72) (left panel) and fluorescent microscopy of GFP signal (right panel), at 24 hpi in ALKBH5-depleted and control cells. GAPDH was used as a loading control. Gel image was cropped to present only relevant proteins. (f) Quantification of viral protein levels from the immunoblot analysis in Fig.1e normalized to the levels of GAPDH. Data are representative of three (d) or two (e) independent experiments.

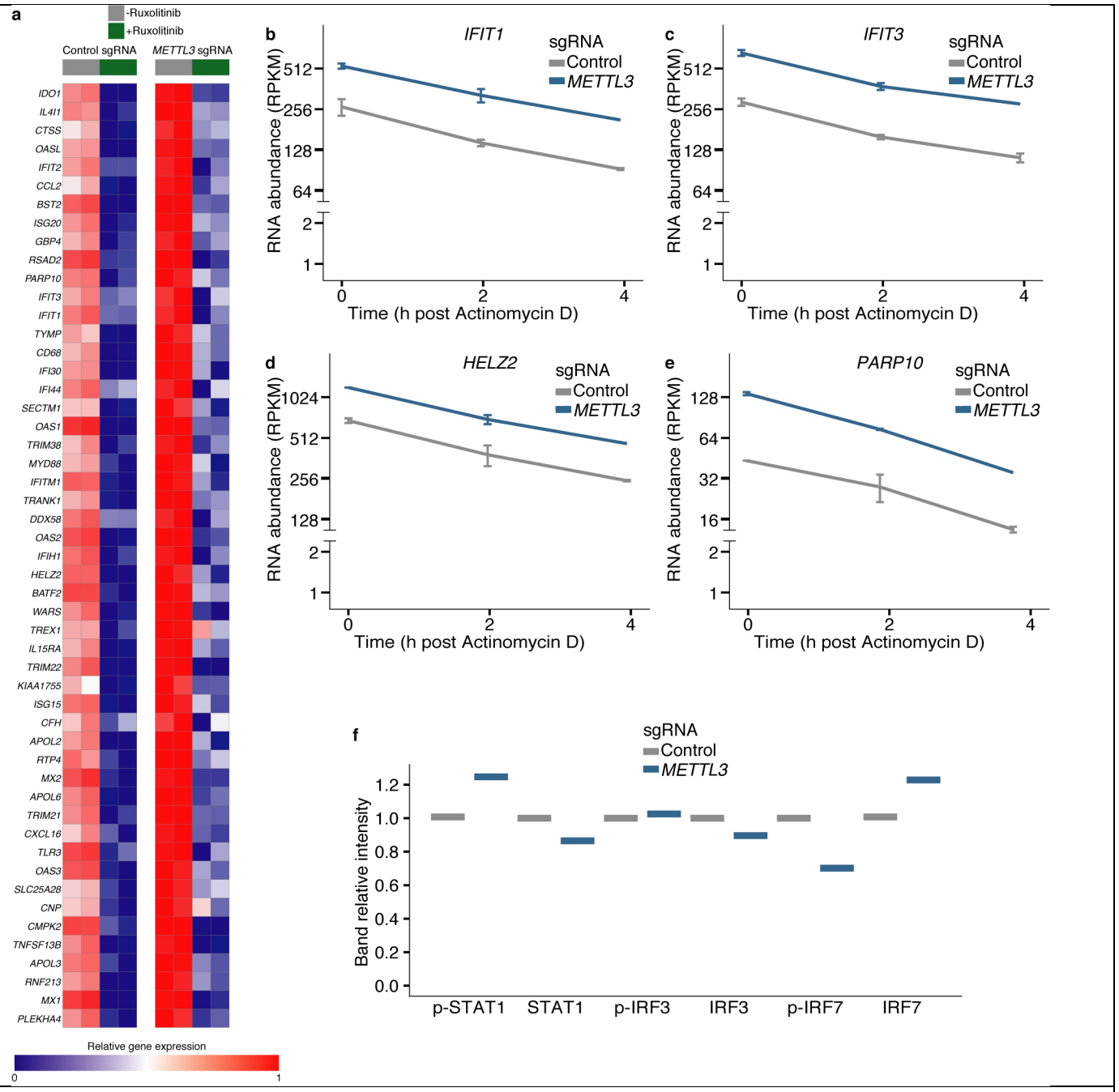

Supplementary Figure 2

Differences in ISG expression between METTL3-depleted and control cells is abolished by Ruxolitinib and does not stem from changes in their stability

(a) ISG relative expression, as measured by RNA-seq, in METTL3-depleted cells versus control cells at 28 hpi, treated or untreated with Ruxolitinib. Expression levels of each transcript were normalized to a scale of 0-1. ISGs showing significant difference (FDR < 0.01) between control and METTL3-depleted cells are presented. (b-e) METTL3-depleted and control cells were treated with Actinomycin D at 22 hpi and harvested for RNA-seq at 0, 2 and 4 hours post treatment. The mRNA decay of several ISGs that showed enhanced expression in METTL3-depleted cells are presented (n = 2 for each time point). Values represent the mean of RNA-seq replicates and error bars show SD. (f) Quantification of protein levels from the immunoblot analysis in Fig.4a normalized to the levels of GAPDH.

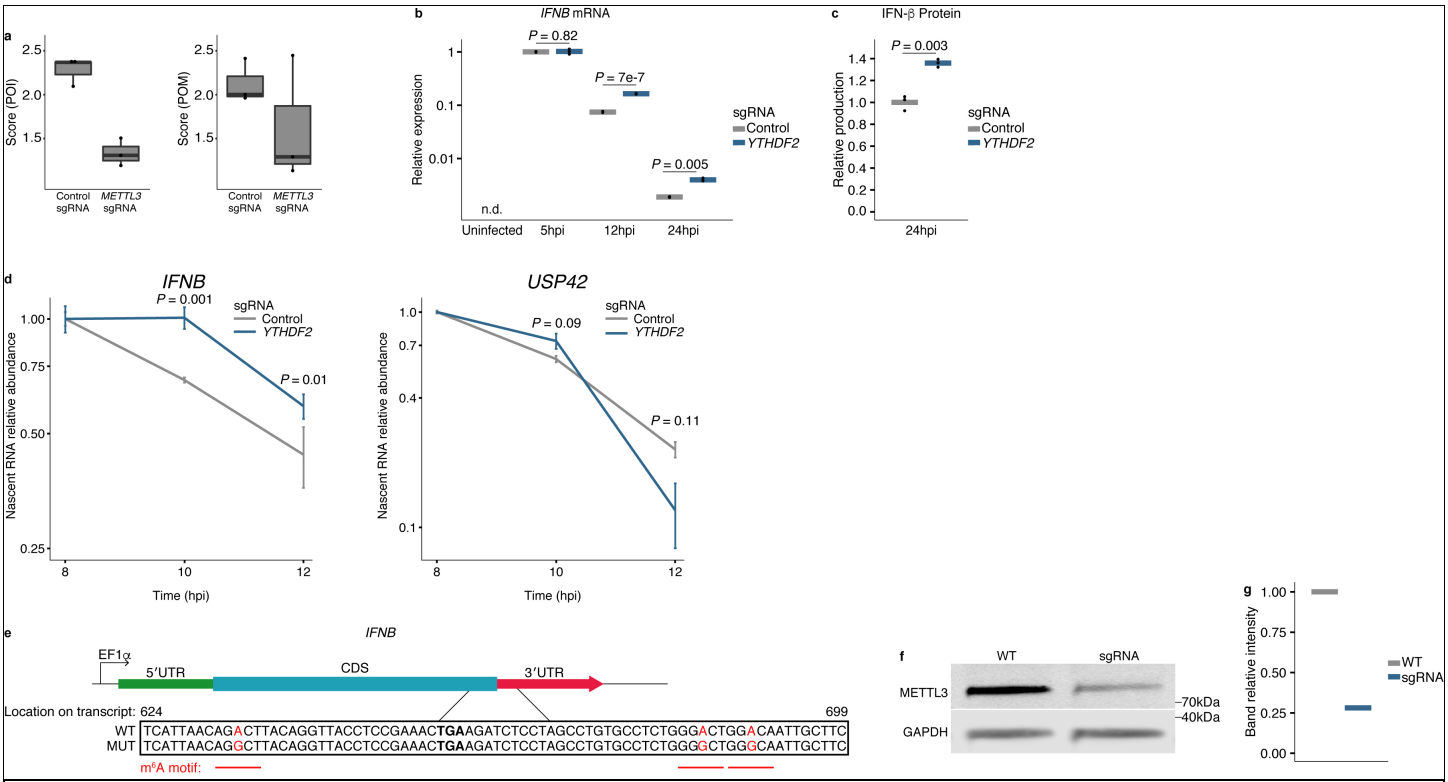

Supplementary Figure 3

IFNB mRNA is m^{6}A-modified and its levels are higher in YTHDF2-depleted cells compared to control cells

(a) Specificity of m^{6}A signal on *IFNB* transcript in immuno-precipitated (IP) samples compared to input (POI, Peak Over Input) and to median coverage across the gene (POM, Peak Over Median), in METTL3-depleted (n = 3) and control cells (n = 3). Thick line, median; box boundaries, 25% and 75% percentiles; whiskers, 1.5-fold interquartile range. (b) *IFNB* mRNA and (c) protein levels in YTHDF2-depleted and control cells at indicated time points post infection, measured by qRT-PCR and ELISA, respectively. *18S* ribosomal RNA was used as a normalizing gene in qRT-PCR. Dots, measurements; bars, mean of three technical (c) and cell culture (d) replicates. *P*-value by two-sided student's t-test. (d) Nascent RNA was labeled for 2 h with 5-Ethynyluridine (EU). EU was washed out and RNA was extracted at the indicated time points. The relative remaining EU-labeled mRNA abundance, normalized to *GAPDH*, was analyzed by qRT-PCR for *IFNB* and *USP42* that was used as control. Values represent the mean of three technical replicates and error bars show SD. *P*-value by two-sided student's t-test. (e) *IFNB* gene (5′UTR, coding sequence and 3′UTR) was cloned into a plasmid in its wild-type (WT) version and in a mutant version (MUT), in which three putative m^{6}A-modified adenosines were mutated to guanosines (labeled in red). (f) Immunoblot analysis of METTL3 in THP1 cells expressing sgRNAs targeting control gene (WT) or METTL3. GAPDH was used as a loading control. Gel image was cropped to present only relevant proteins. (g) Quantification of METTL3 levels from the immunoblot analysis in (f) normalized to the levels of GAPDH. Data (b-d) are representative of two independent experiments.

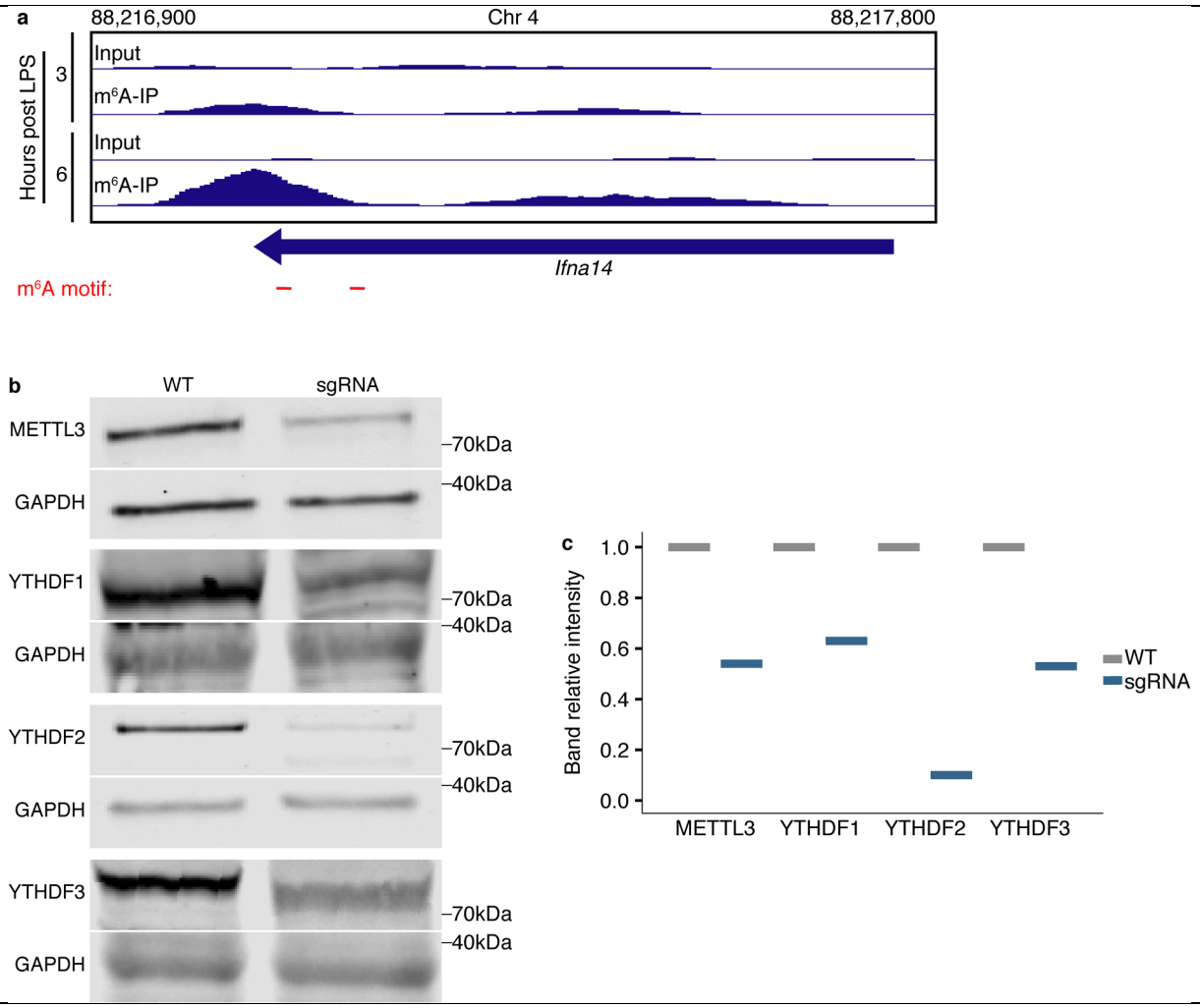

Supplementary Figure 4

m^{6}A-mediated IFN regulation is conserved in mouse

(a) RNA-seq of input RNA and m^{6}A immuno-precipitated RNA from mouse dendritic cells treated with lipopolysaccharide (LPS) for 3 and 6 h is presented for *Ifna14*. (b) Immunoblot analysis of m^{6}A machinery proteins in MEFs expressing sgRNAs targeting control gene (WT) or the various m^{6}A machinery genes (indicated on the left). GAPDH was used as a loading control. Gel image was cropped to present only relevant proteins. (c) Quantification of m^{6}A machinery protein levels from the immunoblot analysis in (b) normalized to the levels of GAPDH.

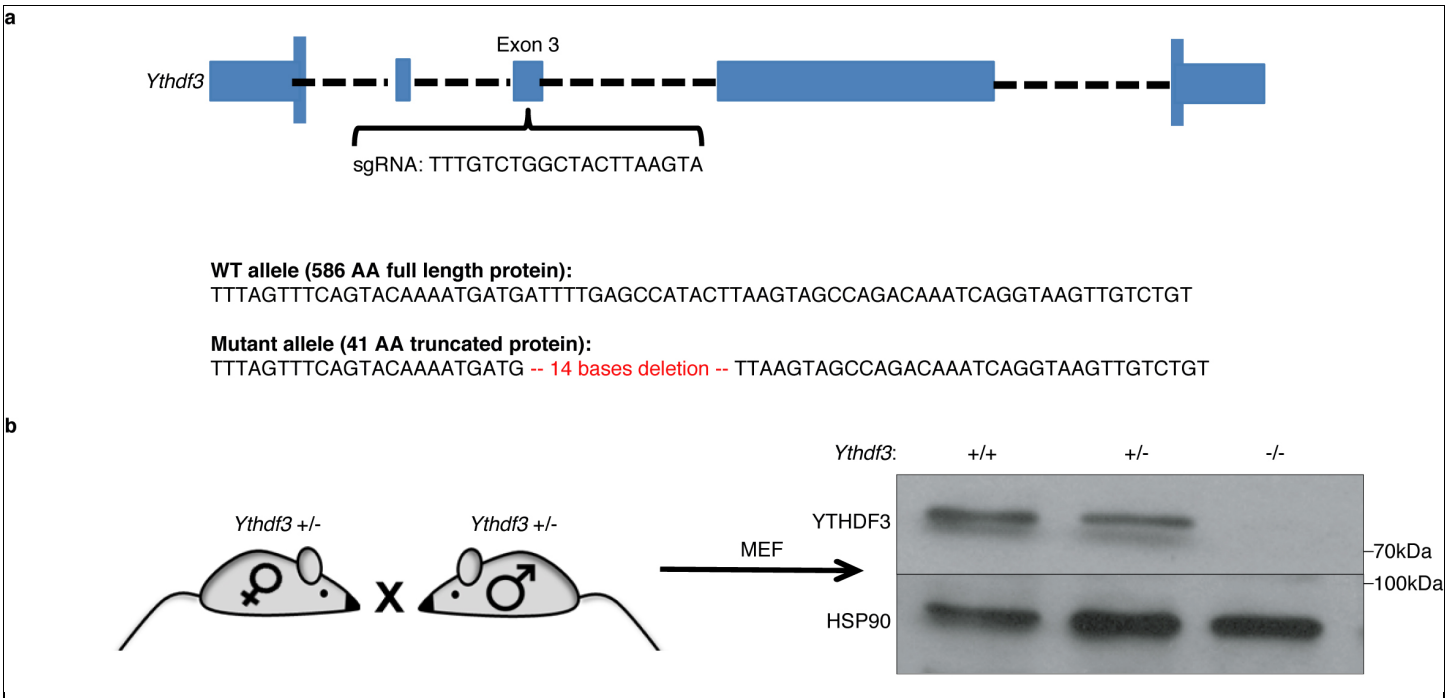

Supplementary Figure 5

Construction of *Ythdf3*$^{-/-}$ mouse

(a) *Ythdf3*$^{-/-}$ mice were generated via one-cell embryo CRISPR/Cas9 injection. sgRNA targeting *Ythdf3* exon3 was used. The mutated *Ythdf3* gene contains an out of frame 14bp deletion, which leads to the production of a stop codon. (b) Immunoblot analysis of YTHDF3 protein expression in MEFs extracted from *Ythdf3*$^{+/+}$, *Ythdf3*$^{+/-}$ and *Ythdf3*$^{-/-}$ embryos. HSP90 was used as a loading control. Gel image was cropped to present only relevant proteins.